Quantum dot/Nanowire Hybrid Nanostructure for Solar Cell Applications

Linda van der Waart
Student number: 1529064

Supervisors:
Dr. Bruno Ehrler, Dr. Erik Garnett (second supervisor),
Prof. Dr. Erik Bakkers (TU Delft supervisor)

Examiners:
Dr. Bruno Ehrler, Prof. Dr. Erik Bakkers, Dr. Jaap Caro, Dr. Gary Steele

Thesis on research for Masters Project (48ECTS)
April-December 2015

Thesis defense: 15 January, 2016

Delft University of Technology
Master Applied Physics
Annotation Sustainability in Technology
Quantum Nanoscience track

Center for Nanophotonics
FOM Institute AMOLF
Amsterdam, The Netherlands

Abstract

The interaction of light and matter at the nanoscale can greatly enhance the absorption of light in photovoltaic devices. In this thesis we combine two components into a hybrid nanostructure to enhance the overall light absorption of an extremely thin absorber: a layer of quantum dots around a nanowire. Quantum dots can be tuned to absorb at very specific wavelengths so that the absorption is perfectly matched to the requirements in the photovoltaic device. Metal nanowires support surface plasmons and can therefore greatly enhance the local optical field, making them ideal counterparts for improved light absorption in the quantum dots. Their ability to ensure efficient carrier collection makes them appealing for solar cell applications. We coated gold nanowires with an average diameter of 100nm with PbS quantum dots of different bandgaps (1.36eV, 0.79eV, 0.61eV) using dithiol linker molecules. A cleaning treatment of the nanowires was essential to remove the nanowire capping agent (PVP) and assure the assembly of a sub-monolayer of quantum dots on the nanowire surface with a coverage of 50%. For high absorption, these nanowires were covered with thicker layers (20nm - 150nm) of quantum dots using a Layer-by-Layer spincoating method. The hybrid nanostructure was characterized using SEM imaging and spatially resolved absorption and photoluminescence. We modeled the interaction of the two systems with Mie Theory and compared this with experimental measurements. As predicted from theory, we observe a redshift of the nanowire resonance with increasing quantum dot layer thickness - at 500nm for uncovered nanowires up to 790nm for nanowires covered with >50nm quantum dots - together with an absorption enhancement. This demonstrates an optical interaction between nanowires and quantum dots. Photoluminescence measurements suggest an electronic interaction between the two, but further research must confirm this. Our results make this highly tunable hybrid nanostructure a promising building block for solar cell applications.

Acknowledgements

Many thanks go out to all the people who helped me finish this thesis. First of all, thanks to Bruno Ehrler for being such a friendly and approachable supervisor. His pleasant, critical and well thought-out feedback during the project helped me finish a piece of work to be proud of. Secondly thanks to both Bruno and Erik Garnett for giving me the opportunity to do my thesis project in their research groups at the AMOLF Institute and providing me with such a professional scientific experience and support. Thanks go out to Erik Bakkers, for being my TU Delft supervisor. I would also want to thank everyone in both the Hybrid Solar Cell Group and the Nanoscale Solar Cell Group. In particular Sander Mann, for providing me with all the theory, helping me with modeling and training me on the optical setup training, Beniamino Sciacca, for helping me with nanowire synthesis and photoluminescence, and being willing to answer all of my endless questions and Le Yang, for providing me with quantum dots and helping me survive in the lab. My acknowledgements to the support staff in the nanocenter, the ICT and the design department at the AMOLF Institute.

Furthermore, I'd like to thank my parents for supporting me during this project, my friends for listening to all my stories about the thesiswork and giving me distraction during my spare time, and finally Nicolai for always being there for me.

Contents

Chapter 1

Introduction

1.1 A hybrid nanostructure for solar cell applications

The sun is an abundant, practically unlimited source of primary energy. Within one hour it can provide enough energy to supply the whole world for a year (see Figure 1.1). Solar cells utilize sunlight as a clean and sustainable way to provide electricity. Yet, most of the suns energy is not being harvested due to the high costs of current solar cell technologies, which represents an economical barrier for the replacement of traditional non-renewable energy sources.

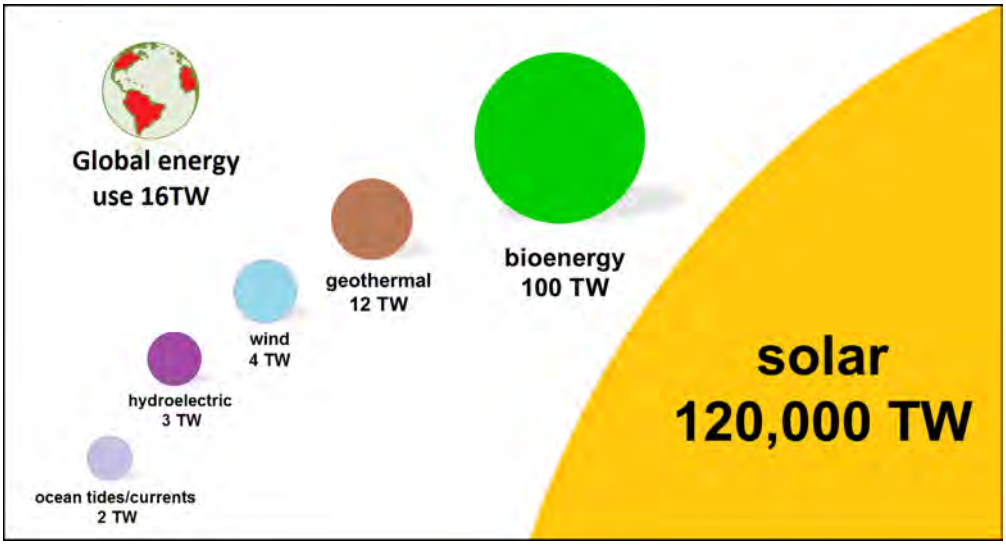

Figure 1.1: **The global renewable energy potential.** Estimate of the renewable energy in TW if sources would be used at their maximum potential. From this image it is clear that the sun outshines the other energy sources. To compare: coal 900TW.

The performance of devices that convert light to electricity ('photovoltaic devices') such as solar cells, is inextricably linked to their capacity for absorbing light. The more of the absorbed light is converted to electricity, the higher the efficiency. Thin-film photovoltaic technologies show promise for achieving efficiencies comparable to conventional silicon solar cells, at lower fabrication costs. Solar cell research often aims at creating high-efficiency thin-film photovoltaic devices for both enhanced efficiencies and drastically reduced material and fabrication costs[1]. To achieve such efficiency improvements, devices must circumvent the Shockley-Queisser limit (a theoretical limit that sets the maximum efficiency of single bandgap systems to 34%) by incorporating novel concepts and device modifications. This includes exploiting techniques like multiple-exciton generation, hot-carrier collection, upconversion and downconversion, by introducing new materials like quantum dots or plasmonic nanophotonic structures[2].

The flourishing field of nanophotonics studies the behaviour of light and its interaction with objects at length scales smaller than its wavelength. Nanophotonics has benefited from the remarkable developments

in the control over the fabrication of materials at the nanoscale. Photovoltaic design approaches based on the manipulation of light at this extremely small length scale can be used to improve light absorption and increase solar cell efficiencies.

In this project, two nanostructures are assembled into a hybrid core-shell nanostructure to enhance light absorption while using little material: quantum dots and metallic nanowires (see Figure 1.2. Quantum dots are nanocrystals that have gained a lot of interest because they enable optimization of their photon absorption to match the solar spectrum. Their unique and tuneable electrical and optical properties make them promising building blocks for photovoltaic devices. However, the highest achieved quantum dot solar cell efficiency is 10.7%[3]. Quantum dot based solar cells are still limited by the trade-off between absorption of light and transport of electrons for providing electricity. Adding more quantum dots would increase photon absorption but results in worse electron transport and therefore a decrease in efficiency. To overcome this problem, we propose the attachment of quantum dots to the surface of a metallic nanowire.

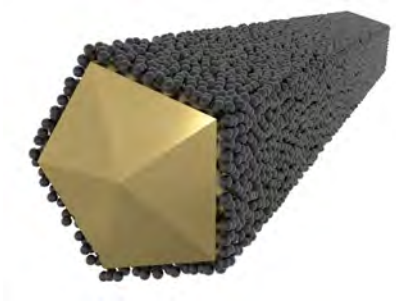

Figure 1.2: **The quantum dot/nanowire hybrid nanostructure as proposed in this project**. Lead-sulfide quantum dots are tunable light absorbers, and by assembling them around a gold metal nanowire that acts as an optical antenna the total absorption in the structure is enhanced without having to use a large amount of material.

Metallic nanowires can concentrate light and when integrated into an absorbing material - in a core shell structure - enhance photon absorption in this material. The shell thickness can be tuned to absorb at wavelenghts corresponding to the solar spectrum. The metal nanowire core can act as a high-performance transparent electrode, making our hybrid nanostructure an ideal building block for solar cell applications[4][5][6]. By proper engineering the dimensions of a gold metal nanowire and coating it with lead-sulfide quantum dots as the photon-absorbing layer, incident light can couple into the hybrid nanostructure to increase the overall absorption in the quantum dots. Since both quantum dots and nanowires are solution processable they are an attractive material for the realization of low-cost, large-area, flexible and lightweight photovoltaic devices[7][8].

1.2 Outline

Background information on solar cells, quantum dots and metal nanowires is provided in Chapter 2. Theoretical treatments used to calculate light absorption in our hybrid nanostructure are introduced. In Chapter 3 experimental methods are presented, from quantum dot and nanowire synthesis, to details about the setup that was used to measure light absorption in single nanoscale structures. In Chapter 4 the results of both the syntheses and the assembly of our new structure are discussed, whereas the results of optical characterization and modeling are discussed in Chapter 5. A final conclusion based on these results will be drawn at the end of this thesis.

Chapter 2

Background

The inspiration for this research-project originates from recent developments in photovoltaic nanoscale technology, where core-shell nanostructures were shown to be promising building blocks in third-generation solar cells[4]. The proposed hybrid nanostructure in this project consists of two components - quantum dots and nanowires - that both show interesting optical and electronic properties and have been succesfully integrated in photovoltaic devices. This chapter provides background information on both quantum dots and nanowires, but first a brief explanation of the basic working principles of a solar cell will be given as a motivation for the project.

2.1 Solar cells and the photovoltaic effect

The 'photovoltaic effect' is the generation of power caused by electromagnetic radiation separating positive and negative charge carriers in an absorbing material. These charges can produce a current for the use in an external circuit, so simply said the photovoltaic effect is the conversion of light (photons) into electricity[9]. In many photovoltaic applications the incoming electromagnetic radiation is solar radiation (sunlight) hence the name 'solar cells'.

The basic principles behind the photovoltaic effect can be divided into four steps: (1) photon absorption, (2) generation of electron-hole pairs (exitons), (3) exciton separation to free carriers and (4) collection of the free carriers at the electrodes (see Figure 2.1)[10].

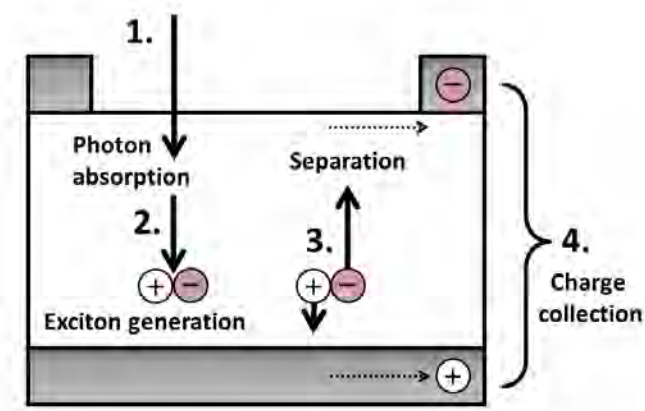

Figure 2.1: **Basic principles of the photovoltaic effect**: a photon gets absorbed by the active material (1) and excites an electron (2) generating an electron-hole pair (exciton). These excitons will then be separated into positive and negative free carriers (3) and collected at the electrodes (4).

The absorbing material in solar cells is a semiconductor material. The photon-absorption in a semiconductor depends on the 'bandgap' of the material: the minimum amount of energy needed to excite an electron from the valence band to the conduction band. This bandgap energy E_G is an energy range in which no electron states exist, and the density of states $\rho(E) = 0$. Since in a semiconductor the Fermi-level energy E_F lies inside this bandgap, all states below the bandgap (the valence band) are filled, whereas the energy states above the bandgap (the conduction band) are available. Simply said, if electrons transfer from the valence band to the conduction band, current can 'flow' through the system.

Photons with energies equal to or higher than the bandgap energy E_G can get absorbed by the semiconductor material, and the bandgap therefore determines the range of photons a solar cell can absorb from the solar spectrum[11]. For an absorbed photon to generate an exciton it has to transfer its energy to an electron by exciting this electron from the valence band to the conduction band. When photons carry more energy than the bandgap-energy, at most an amount equal to the bandgap energy can be used for photovoltaic energy conversion and the excess of energy becomes heat. This sets a limit to the power output of a solar cell since low-bandgap materials absorb more photons and can thus produce large current but at lower energies. In contrast, large-bandgap materials can produce high energy carriers but at lower current due to the limited photon absorption. This trade-off between the output of energy and current requires an optimal choice of bandgap, which is in the range of 1.1 - 1.4 eV (or 880nm-1120nm) in order to have the highest power conversion efficiency in a solar cell containing a single absorbing material[12]. Figure 2.2 pictures this trade-off, assuming there are no losses other than above-bandgap energy loss.

Even though solar cell research and development has extended to various types (and combinations) of materials and device geometries, the basic four steps underlying the working principle of solar cells are the same. So-called 'third generation solar cells' are based on the nanophotonic effect for which the structure size is on the order of the wavelength of light. If the geometrical size of the structure is comparable to

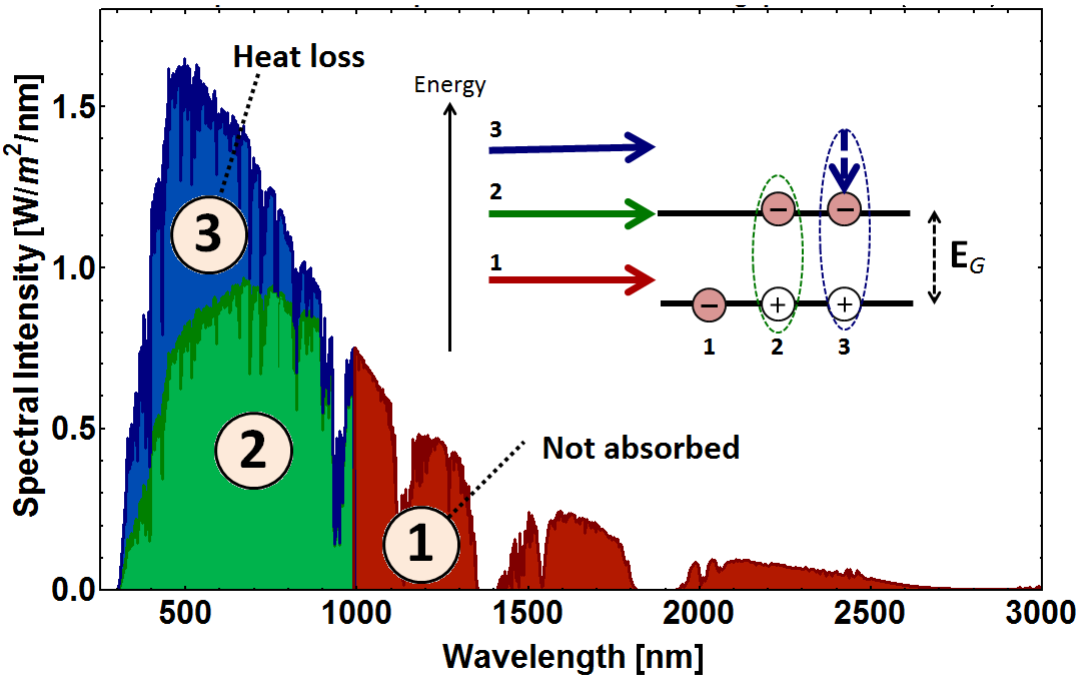

Figure 2.2: **Absorption of photons from the solar spectrum with different wavelenghts in a 1.25eV bandgap material:**. The graph shows the solar spectrum and the colors match the inset with photons of different energies. Photons with energy smaller than the bandgap E_G will not get absorbed and cannot generate an exciton(1), photons with energies equal to (2) or higher than (3) the bandgap will be absorbed by the material and can excite electrons with energies equal to the bandgap energy E_G. In case of (3) the excess of energy will be lost in terms of heat.

the wavelength of light, light can be manipulated and resonant effects can occur that concentrate light, enhancing the photon absorption. These phenomena of light concentration - which will be studied in more detail in the coming sections and in particular in section 2.3 - have opened a new world of photovoltaic research[13].

The next sections will elaborate on the two nanostructures used in this project that are both utilizing nanophotonic effects: quantum dots and nanowires.

2.2 Semiconductor for photon absorption: quantum dots

Quantum dots are semiconductor nanocrystals that have gained considerable interest in photovoltaic research over the past few years[12]. Quantum dots are composed from earth abundant chalcogenides[1], and the possibility to tune the bandgap of quantum dots enables customization and optimization of the absorption profile of this active material to match the solar spectrum. These unique and tuneable electrical and optical properties make quantum dots promising building blocks for optoelectronic devices. Choosing the right chemical environment also gives control over the transport properties of the quantum dots[14]. Since quantum dots are solution processable they are an attractive material for the realization of low-cost, large-area, flexible and lightweight photovoltaic devices[7][8].

[1]Materials composed of an electropositive element with at least one chemical element in group 16 of the periodic table (O,S,Se,Te: a chalcogen anion).

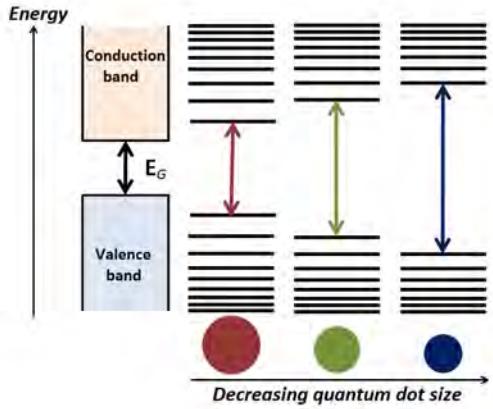

a)

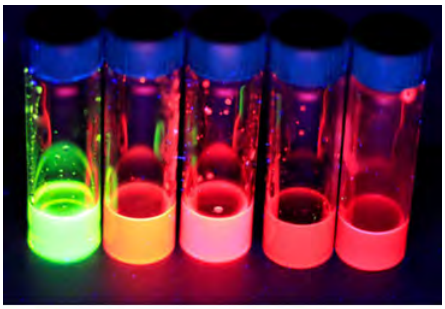

b)

Figure 2.3: **a) Comparison between banddiagrams of bulk material and quantum dots.** Quantum confinement in quantum dots leads to energy band splitting. Just as in a bulk semiconductor material there is a bandgap, but it is tunable with the size of the quantum dot. **b) Bandgap tunability of quantum dots.** Different sizes of quantum dots of the same material have a bandgap at different wavelengths due to quantum confinement. Here the emission of cadmium-telluride quantum dots (*Image used with permission from B. Ehrler*).

2.2.1 Quantum confinement and bandgap

As depicted in section 2.1 an absorbed photon can promote an electron from the valence band into the conduction band of a material, creating an electron hole pair: the exciton. Quantum dots are semiconducting nanometre-scale crystallites that have been reduced below the size of *the natural length scale of the exciton*, or the exciton Bohr radius. When the size of semiconductor structures like quantum dots is similar to or smaller than this exciton Bohr radius, excitons are confined by physical boundaries[15]. The confinement in quantum dots in three dimensions can be approximated by a *spherical particle in a box*, and just as the particle in a box this confinement leads to quantum-size effects, with a splitting of energy levels into a series of discrete electronic transitions - in contrast to the bulk couterpart that shows continuous energy bands[15] (see Figure 2.3). Therefore quantum dots are sometimes referred to as artifical atoms. In reality quantum dots are not perfectly spherical and the particle in a box approximation is not always very accurate[7]. The size of the Bohr Radius compared to the radius of the nanocrystal has influence on the strength of quantum confinement. As the quantum dot size increases and approaches the bulk Bohr radius the energy gap approaches a limit. For PbS quantum dots this limit is the bandgap of PbS bulk material at 0.41eV, and any dot much larger than 20nm in diameter will not be confined and is considered bulk.

Bandgap

Quantum confinement leads to very interesting optical behaviour. The energies of the electron and hole levels are sensitive to the amount of confinement and therefore the optical spectra of the quantum dots strongly depend on the quantum dot size[15]. The energy difference between the lowest available electron state and the highest occupied electron state is the bandgap of the quantum dot. Since we have control over the crystal-growth of the quantum dots, we have control over their size and thus their bandgap. The relation between the PbS quantum dot bandgap E_G in eV and the diameter x in nm is given emperically by the following equation[16]:

$$\Delta E_G^{PbS} = 0.41 + \frac{1eV}{0.0252(x)^2 + 0.283(x)} \tag{2.1}$$

Often bulk bandgaps of chalcogenides are in the near infrared and quantum confinement generally tunes them towards the blue[12]. PbS is a narrow bandgap semiconductor, with a bulk band gap of 0.41 eV, and a large exciton Bohr radius (18 nm), therefore the PbS quantum dot bandgaps can still lay in the infrared, where a large fraction of the solar spectrum is[12].

2.2.2 Exciton generation and transport in quantum dots

In a solar cell, separating the photogenerated exciton and extracting free carriers should happen with as little energy loss as possible. Since quantum dots are very small, a large percentage of their volume is surface area which is possibly creating surface defect states resolving in losses and thus poor charge transport properties[17]. Such defect states act as trapping centers for the photogenerated charges, decrease the charge mobility, enhance recombination, and thereby set a limit to the cell thickness and light-absorption efficiency[17][18][19]. Quantum dots are most often incorporated into solar cells devices by the deposition of layers into a flexible quantum dot film, and the highest achieved quantum dot solar cell efficiency is 10.7%[3]. One of the factors limiting the efficiency of solution-processed quantum dot solar cells is the inefficient charge extraction from the active layer of the device to the electrodes. Charges have to hop from dot to dot in order to be collected[18]. Quantum dots are solution synthesized and are usually capped by stabilising ligands - often by long insulating carbon chains like oleic acid as is depicted in Figure 2.4 - to keep them in solution and avoid aggregation. By changing the chemical environment around the quantum dots after deposition the transport can be enhanced. For example by replacing the long insulating oleic acid ligands to shorter ligands that can function as a binding agent, the electronic coupling between quantum dots is enlarged[14][7].

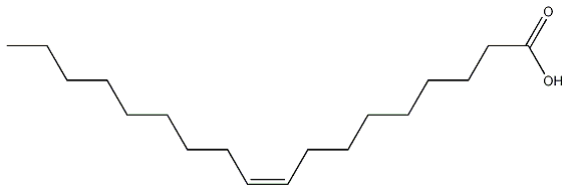

Figure 2.4: **Structural formula of Oleic Acid.** Oleic Acid is often used as the capping agent of PbS quantum dots in octane solution.

Nevertheless a trade-off between the layer thickness and absorption is still present. To facilitate efficient carrier transport the quantum dots-layer must be thin, however this limits the optical path length inside the absorbing material[20]. Even the best quantum dot solar cells are limited by this trade-off. The solution to this problem would be to enhance absorption without using thick layers of quantum dots. In our structure we use a metallic nanowire as an optical antenna to couple more light into the hybrid quantum dot nanowire system.

2.2.3 Multiple Exciton Generation

The Shockley-Quiesser limit for single-junction solar cells is based on the assumption that each photon that is absorbed by a material generates one exciton and that the excess of energy above the bandgap is lost[21]. A process in which two or more excitons are formed from one absorbed photon would overcome this limit. Such a process has been demonstrated for the first time in PbSe quantum dots in 2004 by Klimov and Schaller, and was later named 'Multiple Exciton Generation' (MEG)[22]. Figure 2.5 depicts the MEG in a simple manner. The idea of creating multiple excitons from one electron had been researched for years in bulk materials, but deemed too inefficient for solar cell applications. Quantum dots offer more efficient MEG than bulk materials[23]. In 2010 MEG has been proven in PbS quantum dots and one year later PbSe quantum dot solar cells have been published with an EQE (the ratio of extracted electrons to incoming photons) of over 100%[24][25]. The possibility to overcome efficiency limits with MEG is one of the interesting and promising properties of quantum dots for solar cell applications.

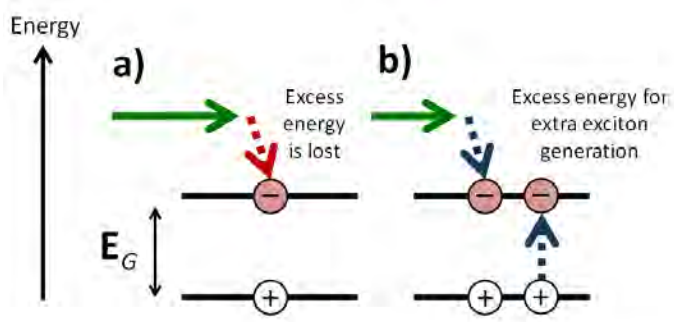

Figure 2.5: **Multiple Exciton Generation (MEG):** The green arrow depicts an incoming photon with above bandgap energy. In (a) the excess of energy is lost while in (b) the excess of energy is used for the excitation of a second electron, generating multiple excitons from only one photon.

2.3 Resonators for absorption enhancement: metal nanowires

Metallic nanostructures have been shown to be promising building blocks for photovoltaic devices because they efficiently concentrate light and enhance absorption in a variety of photovoltaic materials due to surface plasmon resonances (SPRs): collective oscillations of free electrons at a metal/dielectric interface that occur during optical excitation. In an asymmetric structure like a nanowire or a nanorod these oscillations can occur either along its long axis (which we call 'TM polarized') or perpendicular to its long axis ('TE polarized'), as is depicted in Figure 2.6. A TM polarized SPR is generally not present in nanowires because their length exceeds the wavelength of light. The resonances can be adjusted to the solar spectrum by modifying the nanowire geometry and changing its surrounding material, making the structure highly tunable.

Plasmonic structures

Nanometallic (or plasmonic) structures have the ability to concentrate and manipulate light at the nanometre scale due to their ability to support SPRs[26]. Because of the small size of nanostructures, resonant modes can interact with the environment[27]. This 'optical antenna effect' means that the area in which light is manipulated by a nanostructure becomes bigger than the actual size (or geometrical cross section) of the nanostructure, which can cause strong light absorption in the vicinity of the nanostructure[28]. Figure 2.6 (d) shows the 'antenna effect'.

The SPR depends strongly on the intrinsic properties and the geometry of the material, and the light-trapping effects are most evident at the peak of the resonance spectrum, which can be tuned by engineering the nanowire diameter and the dielectric constant of the surrounding medium[13].

Metal nanowires are particularly interesting for integration into photovoltaic structures as they allow for charge extraction and could function as a (local) contact for the collection of free carriers[4]. Metal nanowire networks have been shown to achieve excellent transport properties as transparent electrodes[29] even on large scale[20]. The fact that nanowires are solution processable makes them appealing for low-cost application on large-scale[30].

2.4 Core-shell hybrid nanostructure

The medium surrounding the plasmonic nanoparticles is an important factor of the SPR wavelength and thus of the light absorption. Gold nanowires with 100nm diameter show a resonance peak at around 500nm when surrounded by air, but this redshifts when surrounded by materials with a higher dielectric. When two structures are combined in a core-shell geometry - by wrapping a shell around a nanostructure - it is possible to enhance the absorption in the overall system. The thickness of this shell is an important factor. Zhan et al. showed that the photon absorption in a single nanowire could be enhanced by wrapping a semiconductor shell around a silver nanowire[31]) and Mann et al. showed that a *very* thin

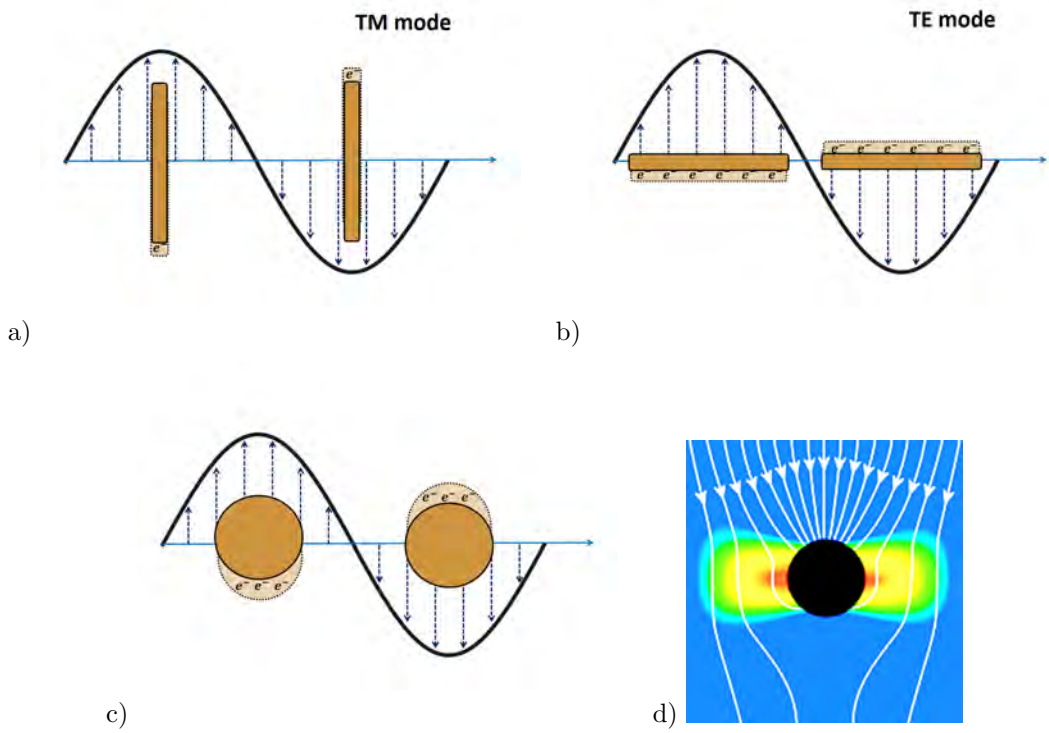

Figure 2.6: **(a),(b) Surface plasmon resonances in a metal nanowire**. Light enters a nanostructure and the polarization of the electric field gives rise to either a resonance along the nanowire axis ('TM polarized') or perpendicular to the nanowire axis ('TE polarized'). The length of nanowires is in reality much larger than the wavelength of light and a TM mode is not appearent. TM modes do appear in nanorods (smaller lengths). **(c) An image of surface plasmon resonances in a metal nanoparticle. (d) The antenna effect:** a horizontally polarized surface plasmon resonance in a metallic nanoparticle (black sphere) gives rise to high induced electric field (density plot, red is high field) resulting in the concentration of light, where the white arrows depict the pointing vector (flux) of the propagating photons. *Image used by the permission of A. Polman.*

shell around a metallic nanowire could increase the absorption extremely, by increasing the strength and number of resonances apparent in the core-shell system[4]. Both conclusions were drawn from theoretical modeling by the use of Mie Theory.

2.4.1 Mie Theory

In 1908, Gustav Mie introduced a theory in an effort to better understand why different sizes of gold nanoparticles in solution colored the solutions differenly. This phenomenon is known for over hundreds of years, and images of old stained glass in churches, or drinking cups aging from the Roman times (see Figure 2.7) are often used to demonstrate this 'nanotechnological' effect[32].

In essence, Mie provided a description of light scattering from a nanospherical particle of arbitrary material. He started with the Maxwells equations and by decomposing the incident, scattered and internal electromagnetic fields into a basis set of vector spherical harmonics, the electromagnetic field inside and outside of the particle could be mathematically represented by a series of functions that are solutions to the Maxwell equations[33].

Mie Theory can be used to model SPRs in for example nanospheres or nanowires, but also in core-shell structures. We used Mie Theory in this project as a well known tool to theoretically analyze what happens with the optical properties of an (infinitely long) metal nanowire when quantum dots are packed around it. Below a simple introduction into Mie Theory calculations is given. For any details on the calculations and the governing equations for this theory on electromagnetic fields and boundary conditions we refer

Figure 2.7: **(a) The Lycurgus cup.** When lit from the front the cup appears green. However when lit from the rear, the cup appears red. This change in colors is explained by light scattering of nanoparticles in the glas. *Trustee of the British Museum.*

to the book by Bohren and Huffman[34].

Start with incoming light as a plane electromagnetic wave with a wavelength λ incident on a nanoparticle of some radius r with a complex refractive index. The interaction between the nanoparticle and the incoming light causes the sphere to radiate electromagnetic waves off itself, which can be represented mathematically by expanding this outgoing wave using vector spherical harmonics, which involves Legendre polynomials and Bessel functions. The solutions to this expansion includes expansion coefficients, or also called 'Mie coefficients' and are often written as a_n and b_n, where n is the expansion index going from $n = 1$ to $n \to \infty$. These coefficients are build up from Bessel functions and include the refractive indices of the nanostructure and its surrounding medium. The incoming wave can also be expanded into spherical harmonics again with expansion coefficients (say c_n and d_n) and the interaction between the incoming and outgoing waves can be understood by solving the Maxwell equations applying the right boundary conditions. With these Mie coefficients the so called scattering cross section C_{sca} and extinction cross section C_{ext} can be calculated and by substracting C_{sca} from C_{ext} the absorption cross sections C_{abs} is computed:

$$C_{sca} = \frac{2}{kr^2} \sum_{n=1}^{\infty} (2n+1)(|a_n|^2 + |b_n|^2) \tag{2.2}$$

$$C_{ext} = \frac{2}{kr^2} \sum_{n=1}^{\infty} (2n+1)\mathrm{Re}(a_n + b_n) \tag{2.3}$$

$$C_{abs} = C_{ext} - C_{sca} \tag{2.4}$$

with r the radius of the nanoparticle, k the wavevector of the light and a_n and b_n the Mie coefficients. The absorption cross section is the total amount of energy removed from the electromagnetic wave due to absorption divided by the power density (flux) of the incoming wave. Therefore an absorption (or scattering or extinction) cross section is in m^2 (or often in $\mu\mathrm{m}^2$). It is also referred to as a 'probability for absorption'. The absorption efficiency η_{abs} is found from division of the absorption cross section by the geometrical cross section of the nanostructure $\frac{C_{abs}}{C_{geo}}$, which can exceed 1 because of the antenna effect at the nanoscale.

These values of refractive indices are found in the Handbook of Palik[35] or can be measured. The solutions to the equations according to Mie Theory are very much dependent on the particle size and the medium of both the particle and its surroundings.

2.4.2 Ligands: gluing the structures together and tune the properties

Linker molecules were used to 'glue' the quantum dots onto the gold nanowire creating our hybrid nanostructure. These linker molecules or ligands assure an electronic connection between the two structures if

they bind to both the nanowire and quantum dots, doubling as a bridge for charge transfer between the two. We chose dithiols as linker molecules. The dithiols we use are called (alkane)thiols: molecules with an alkane chain (a $(C\text{-}C)^n$ chain), a tail group and an S-H head group. Dithiols have an alkane chain with on both ends an S-H group as seen in Figure 2.8. Other types of alkanethiols include aromatic thiols, in which the alkane chain is (partly) replaced by benzene rings. Thiols show the possibility of linking to metals via the strong affinity of sulfur to covalently bind to metals. Thiols are also most commonly used for creating Self Assembled Monolayers (SAMs)[2]. SAMs provide a useful system with which to accommodate the surface properties of several materials like metals, metaloxides and semiconductors and have been researched thoroughly[36]. Also, dithiols have been used as linker molecules between quantum dot layers in solar cells, as described in section 2.2.2.

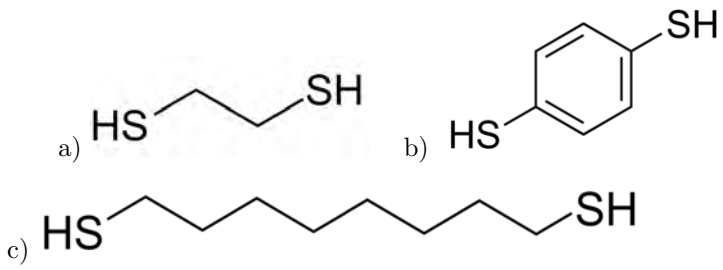

Figure 2.8: **(a) Structural formula of different types of dithiol molecules.** (a) 1,2-Ethanedithiol, (b) 1,4-Benzenedithiol and (c) 1,8-Octanedithiol.

In this project gold nanowires were used as the metallic nanostructure. According to Love et al. there are good reasons to use gold as a standard surface on which to grow SAMs. The first is that SAMs formed with (di)thiols on gold are stable for long periods, at least weeks. Another reason is that gold is the most studied metal for SAMs, and gold is easy to obtain in different geometries. Finally, gold is a reasonably inert metal, meaning there are fewer problems with chemical reactions like oxidation compared to for example silver[36].

2.5 Summary

The highly tunable core-shell quantum dot nanowire hybrid nanostructure shows promising benefits as a building block for photovoltaic devices. The quantum-size effect appearing in quantum dots opens the possibility of creating artificial solids with tunable electrical and optical properties and the possibility of MEG offers advantages over conventional semiconductor materials[37]. Yet, a challenge lies in enhancing the absorption of quantum dots films, since the small size of quantum dots introduces a lot of surface area and thus many possible recombination traps which decrease their transport properties. The trade-off between thick layers to absorb all of the above band gap photons and thin layers for efficient carriers transport can be solved by introducing a plasmonic nanowire, which has the ability to manipulate and concentrate light at the nanometre scale to enhance absorption due to its ability to support SPRs. These resonances can be tuned by changing the nanowire material and diameter, and by changing the dielectric of its surrounding medium. By the use of Mie Theory, core-shell structures have been shown to enhance photon absorption because they also support resonances. Dithiols can be used to glue the quantum dots as a shell around the nanowire. SH groups at the end of dithiols both show affinity to PbS quantum dots and gold, and can function as the linker molecules between the two materials. Since different types of dithiols have been shown to increase transport properties in quantum dot films, they can give us control over the electronic properties of this hybrid nanostructure. Because the metal nanowire allows for charge transport and can function as one electrode, introducing a second electrode could allow for charge collection, making the hybrid nanostructure interesting for solar cell applications.

[2]SAMs of organic molecules are molecular assemblies that can be formed spontaneously in ordered domains on surfaces by adsorption.

Chapter 3

Methods

This chapter explains the research methods used in the project. The first part of this chapter describes the fabrication of the samples and involves chemical details. PbS quantum dots were synthesized and characterized, gold nanowires were synthesized and characterized and then these two components were assembled in a core-shell hybrid nanostructure. In the second part of this chapter measurement equipment to characterize the hybrid nanostructure is explained in more detail. The chapter finishes with details on the interpretation of both the theoretical and experimental data.

Table 3.1: Table with chemicals used in the chemical processing and cleaning, their abbreviations and purchase-details.

Material/Chemical	Abbreviation	Details
Quantum dots		
Lead(II) chloride	$PbCl_2$	powder, 98%
Bis(trimethylsilyl) sulfide	TMS_2S	$\geq$ 98%
Oleylamine	OLA	technical grade, 90%
Oleic Acid	OA	$\geq$ 99%
Lead(II) oxide	PbO	99.999%
1-Octadecene	ODE	technical grade, 90%
Trioctylphosphine	TOP	97%
Diphenylphosphine	DDP	98%
Nanowires		
Gold(III)Chloride Hydrate	$HAuCl_4$	99.999%, trace metals basis, $HAuCl_4.xH_2O$
Tetraethylene Glycol	TEG	99%
Poly(vinylpyrrolidone)	PVP	powder
Dithiols for functionalization		
1,2-Ethanedithiol	12EDT	$\geq$ 98%
1,3-Benzenedithiol	13BDT	99%
1,4-Benzenedithiol	14BDT	99%
1,4-Butanedithiol	14BuDT	97%
1,8-Octanedithiol	18ODT	$\geq$ 97%
Chemical cleaning		
Aqua Regia		
Hydrochloric Acid	HCL	ACS reagent[1],37%
Nitric Acid	HNO_3	ACS reagent,70%
Base piranha		
Ammonium hydroxide	NH_4OH	ACS reagent 28.0 - 30.0%
Hydrogen peroxide solution	H_2O_2	puriss. p.a. $\geq$ 30%
Typical solvents		
Acetone	ACE	Ethanol AR[2]
Acetonitrile	ACN	Acetonitrile AR
Ethanol	EtOH	Ethanol absolute (Dehydrated) AR
Methanol	MeOH	Methanol absolute AR
Isopropanol	IPA	2-Propanol AR
Deionized water	DI-water	

All chemical reactions took place in a fumehood at room temperature unless stated otherwise. Typical solvents used were purchased from Biosolve Chemicals. All other chemicals used for the synthesis of PbS quantum dots and gold nanowires were purchased from Sigma Aldrich and were used as received. The abbrevations for the chemicals can be found in Table 3.1. Glassware for experiments was purchased from VWR and glassware for storage came from Supelco (Sigma Aldrich). Tubes used for centrifugion and storage were standard 15ml plastic centrifugation tubes.

[1]ACS reagent: the chemical conforms to specifications defined by the Committee on Analytical Reagents of the American Chemical Society.

[2]AR: Analytical grade solvent and reagent.

Cleaning substrates for sample preparation

Silicon pieces with areas of 0.5-1cm^2 were used as substrates for imaging. They were plasma-cleaned with oxygen before use, adding a SiO_2 toplayer on the silicon. Because this toplayer is very thin and does not last long, we refer to the silicon/SiO_2 substrates as 'Si'. Microscope glass slides were cut in 65x7.9x1.5mm and marked by the aid of a diamond scraper. Both the Si and the glass substrates were cleaned before use by sonication for 10 minutes in IPA. Then the substrates were washed with DI-water and blown dry with nitrogen.

3.1 PbS quantum dot synthesis

Cold injection method

The synthesis of PbS quantum dots was a modified version of previously reported methods by Zhang et al[38]. Figure 3.1 (a) shows a cartoon of the setup. Two 3-neck-flasks were cleaned with ACE and IPA, equipped with a temperature probe and a teflon stirring bar, put on a hotplate and connected to a Schlenk line by the use of grease. OLA (8ml) and 3mmol $PbCl_2$ (0.834 grams) were degassed under vacuum by heating slowly to 80°C and maintained at this temperature for 30mins, stirring at 400rpm. While increasing the temperature to 80°C, caution must be taken not to have bubbles touching the grease and contaminating the solution. Then the solution was allowed to cool below 30°C and placed under nitrogen.
Separately, 20ml of OLA was degassed by heating slowly to 80°C under vacuum, and then placed under nitrogen. The sulfur precursor was prepared in a glovebox by dissolving 210μl of TMS_2S in 1 ml of the degassed OLA. The degassed Pb-oleate solution was reheated slowly under stirring and when at 30°C, the sulfur precursor was rapidly injected. When at 90°C (after ± 1 min), 10ml of hexane was quickly injected to stop the crystal growth and the solution was slowly cooled down to RT by removing the flask from the hotplate. When cooled down, the solution was transferred to several tubes and IPA was added in a 1:1 proportion for purification. A 'crash' was prepared by the addition of MeOH until the solution became cloudy (often 1ml per 10ml). After centrifugating the supernatant for 5min at 5000rpm (Hettichlab Universal-320 Centrifuge) the precipitate was disposed off and the synhtesized quantum dots were dried in an open tube for 24h in a fume hood. Then octante and OA were added in a 4:1 proportion to replace the weakly bound OLA ligands by OA, and stored for 24h. Another crash was prepared (IPA in 1:1 proportion, then MeOH), the quantum dots were dried, octane was added and the solution was filtered (acrodisc CR 13 mm syringe filter, Pall) by the use of a syringe (Sterican and Injekt, Braun). The solution with OA capped quantum dots was stored in a closed vial in a fume hood (see Figure 3.1 (b)).

Hot injection method

The hot injection method was done by Le Yang, and previously reported[40]. It is similar to the synthesis described in the previous section, but with some changes: PbO (2.0 mmol, 0.45g) and OA (4.73 mmol, 1.5ml) were dissolved in ODE (62.5 mmol, 20ml) and degassed under vacuum at 100°C. TMS_2 (1.0 mmol,213μl) and DPP (0.60 mmol, 104μl) were degassed in degassed ODE (31.25 mmol, 10 ml) to prepare the precursor mixture, which was injected rapidly into the reaction mixture at 120 - 170°C under nitrogen. The heating mantle was removed and the flask was subsequently allowed to cool to 35°C. Purification steps were performed under inert atmosphere via repeated cycles of dissolving the hexane, and precipitation with an ethanol or 1-butanol/methanol mixture. Then the PbS quantum dots were re-dissolved in octane and stored in a vial in a fumehood.

Determination of quantum dot concentration

The quantum dot mass concentrations were measured gravimetrically by drying 50μl quantum dot-solution on a microscope glass slide. The weight before and after the quantum dot addition was taken several times on a balance with accuracy of 10^{-4}g (Denver Instruments SI-234).

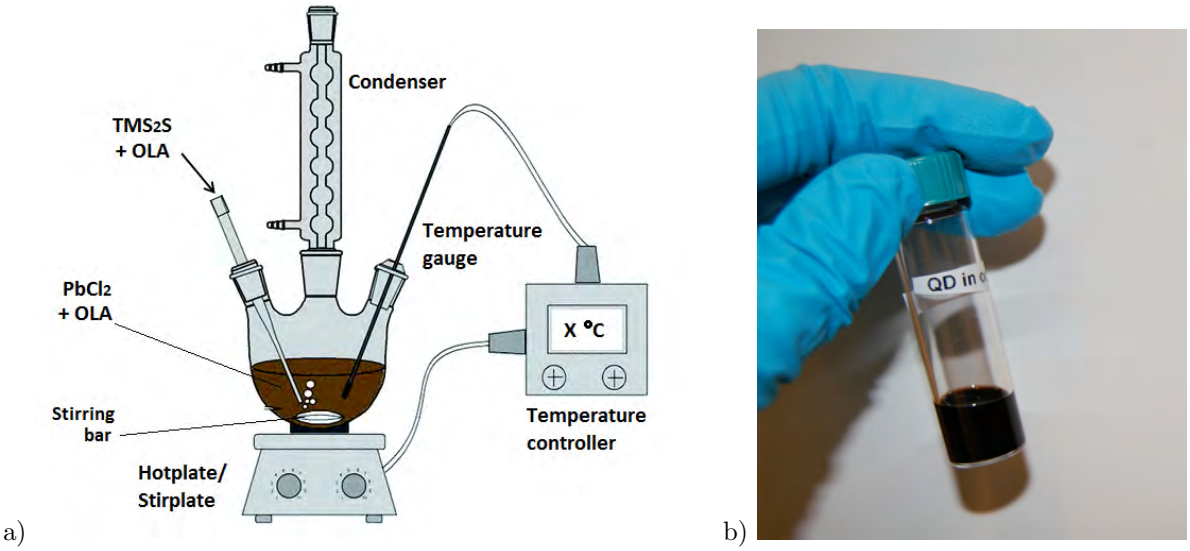

Figure 3.1: **(a) Schematic image of the setup used for the cold-injection synthesis of PbS quantum dots:** A 3-neck-flask was equipped with a temperature gauge and a teflon stirring bar, put on a hotplate/stir plate and connected to a Schlenk line via a condensor. TMS_2S in degassed OLA was added to $PbCl_2$ in degassed OLA and heated while stirring and placed under nitrogen. Image based on [39].**(b) Vial with quantum dots**. The quantum dots absorb in the visible and the infrared so they have a black/brown color.

UV-Vis spectroscopy

The absorbance of synthesized quantum dots was measured in octane solution with a UV-Vis spectrometer (Perkin Elmer UV/VIS/NIR lambda 750). Three cuvettes (10 mm standard quartz cuvette, Spectral Analysis) were cleaned and rinsed with octane. Two cuvettes were filled with octane only and one with quantum dots in octane (for example add 5μl of 25mg/ml QDs to 5 milliliter of octane: make sure to see a slight color change after quantum dot addition).

Ellipsometry

Ellipsometry measurements were done on films with a 100nm thick layer of PbS quantum dots spin-coated on Si wafers with a VB-400 Variable Angle Spectroscopic Ellipsometre (Woollam) using monochromatic light from a xenon lamp guided through a monochromator. The refractive index was determined by fitting the data with a Cauchy and a Gaussian model. The measurement was fitted into an optical model by using a point-by-point fit and subsequently a normal fit to generate a set of Kramers-Kronig consistent refractive indices (n) and extinction coefficients (k) over a wavelength range of 300-1700nm.

3.2 Gold nanowires synthesis

The synthesis of gold nanowires was based on previously reported methods by Seo et al. where gold decahedrons were used for an anisotropic growth of Au nanowires [30][41]. The gold decahedrons were synthesized by Beniamino Sciacca and stored in EtOH suspension in the fridge.

Cleaning glassware

All the glassware used for this synthesis was cleaned with Aqua Regia (for details on the chemical cleaning components, see Table 3.1). Aqua Regia is a highly corrosive mixture of acids (3:1 volume ratio of HCL and HNO_3). A 25ml round bottom flask including a teflon stirring bar and a 10ml vial were cleaned as follows: 30ml HCL was poored in a 50ml beaker, then 10ml HNO_3 was added. The components must always be mixed in this order. Then the Aqua Regia was poured into the glassware, with the flask

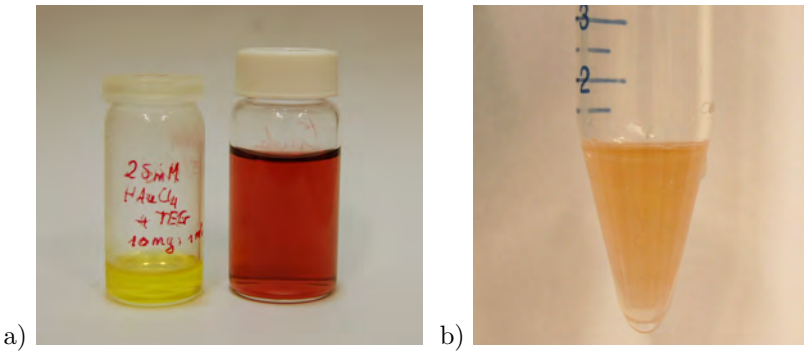

Figure 3.2: **(a) Components used in the nanowire synthesis:** left vial holds Gold(III)Chloride Hydrate. Its fluorescent yellow color dominates the color of the nanowire suspension for the first few hours. Right vial: the gold decahedron seeds, with a bright reddish color. **(b) Gold nanowires in EtOH**: to note the presence of nanowires, the suspension must appear 'cloudy' when shaking the tube.

containing the stirring bar, and kept in glassware for 30-60min. The color changed from yellow to darker yellow/orange. For the disposal of Aqua Regia, the Aqua Regia was slowly added to a 1:5 proportion of DI-water, in our case 200ml. The components must always be mixed in this order. The glassware was filled three times with DI-water and all was disposed of in an acidic waste container. Then the glassware was rinsed five times with DI-water. The glassware was dried and stored in an oven.

Growth of gold nanowires from gold decahedrons

1g of PVP (Mw 55.000 and Mw 360.000 were both tried) was added in small amounts to 15ml TEG in round bottom flask with stirring bar. Heating, stirring and sonication for hours was needed to fully dissolve the PVP. Then the flask was placed in an oil bath under permanent stirring at 400rpm at 100°C and 300μl gold decahedrons in EtOH were added (13μmol with respect to the gold precursor concentration[41]). 1ml of 25mM $HAuCl_4$ in TEG was added, and the resulting mixture was heated to 100°C at 300rpm and kept at this temperature for 24-30 hours. Since the solution was very viscous, caution had to be taken to check whether the solution was stirring properly. The color changed from bright yellow, to purple (after 5h), to gold. Then the nanowire suspension was cooled down to RT and poured into several tubes. Some milliliters of ACE was added to dilute the viscous TEG and the suspension was centrifuged for 10min at 6000rpm (Hettichlab Universal-320 Centrifuge). The precipitate was disposed of, ACE was added and the suspension was centrifuged again. This step was repeated with DI-water instead of ACE, and then repeated with EtOH instead of DI-water. The last step with EtOH was repeated several times until the TEG was removed and the nanowires were fully dispersed in EtOH. The nanowires were stored in EtOH (capped by PVP) at RT in air. Before characterization or further processing, the suspension was always stirred and sonicated in order to re-disperse the nanowires. See Figure 3.2 for components of the reaction and the obtained nanowires in EtOH suspension.

3.3 Functionalization and assembly without PVP removal

Several approaches were taken to attach the quantum dots on the nanowire surfaces, where we can distinguish between methods with and without a PVP removal before assembly. This section will discuss the approaches without PVP removal and the next section will discuss similar approaches with the removal of PVP.

Functionalize quantum dots in solution

100 μl quantum dots were functionalized with 100μl 14BuDT (10mM in octane) in 3ml octane. After 3 and after 24 hours they were cleaned by centrifugion, filtered (acrodisc CR 13 mm syringe filter, Pall) and transferred to EtOH. 3h functionalizing led to clustering, but after 24h the as obtained solution was

sonicated, filtered and the solution looked transparent. The functionalized quantum dots were stored in an EtOH solution.

Assembly

Three approaches were taken to assemble nanowires and functionalized quantum dots.

1. 10μl 14BuDT-functionalized nanowires were dropcasted on Si substrate and placed in 500μl 14BuDT-functionalized quantum dot solution
2. 10μl 14BuDT-functionalized quantum dots were dropcasted on Si substrate and placed in 50μl nanowires (14BuDT-functionalized) in 500μl EtOH suspension
3. 50μl 14BuDT-functionalized nanowires were added to 14BuDT-functionalized quantum dot in 500μl EtOH. Then dropcasted on Si.

The substrates were cleaned by gently shaking in octane and keeping in ACE and IPA for 30 seconds, and stored in a sample box in air.

Functionalize nanowires in EtOH/octane suspension

In order to replace the PVP capping ligands around the gold nanowires by dithiols, an attempt to do this functionalization was done in suspension, both in EtOH and in octane. 10mM of various dithiol-solutions (12EDT, 13BDT, 14BuDT, 14BDT, 18ODT) were prepared by adding dithiol to EtOH/octane after which the mixture was placed under bath sonication for 15 minutes. 300μl of the nanowire suspension in EtOH/octane was put in 10ml EtOH/octane together with 1ml 10mM dithiol solution, and a teflon stirring bar was added. The suspension was stirred at 400rpm for times ranging from 24-72h. Nanowires were centrifuged at least three times for 5min at 6000rpm, redispersed in either EtOH or octane, and stored in a tube in air.

Functionalize nanowires in solid state

5 or 10μl nanowires were dropcasted on a Si substrate and dried. The sample was then placed in a 1-3mM dithiol-solution, either in EtOH or octane for 24-72h. Then the samples were taken out of dithiol solution, washed in EtOH and stored in EtOH solution.

Assembly

The nanowires functionalized in solution were dropcast on a Si substrate and brought in contact with quantum dots. Also the nanowires functionalized on a substrate were brought in contact with quantum dots, either by dropcasting quantum dots from solution on the substrate and dry at RT or in the fridge to slow down the evaporation of the quantum dot solvent, or by putting the substrate in a quantum dot-solution for times ranging from 1min-24h. Some samples were placed in quantum dot solution either at RT or after a 24h heating at 100°C. Then the substrates were cleaned by shaking in octane and holding for 30 seconds in ACE and IPA, and stored in a sample box in air.

3.4 Functionalization and assembly with PVP removal

5-10μl of gold nanowires were dropcast from suspension on a cleaned substrate (Si or glass). They were dried and stored in a sample box untill further cleaning steps. Both the cleaning and the functionalization took place in a cleanroom (ISO class 5) in order to avoid any cross-contamination with other particles.

Cleaning the gold nanowires with O_2-Plasma

The substrates were plasma cleaned for PVP removal for 1, 3, 5 or 10 minutes in an Oxford Plasmalab 80+ Ion beam etcher, via an O_2-plasma treatment operating at 50W Forward Power, 200V DC Bias, 20°C Chamber Temperature, 25sccm O_2 under 5mTorr pressure.

Figure 3.3: **The 5 step cleaning process.** Substrates were taken out from quantum dot solution and held in 15ml octane (1) to wash off the excess of quantum dots. Then the substrate was transferred to a second vial with 15ml octane (2) and moved sturdy to remove any unbound quantum dot leftovers. The substrate was then kept in ACE (3) and IPA (4) for 30s, and blown dry with a nitrogen-gun (5).

Cleaning the gold nanowires with Base piranha

The substrates were chemically cleaned with base piranha (5:1:1 proportion of DI-water:NH_4OH:H_2O_2). For safety precautions organic solvents like IPA must be kept separaely from base piranha. Samples were placed in a teflon sample basket. A beaker was filled with 5 parts DI-water and 1 part NH_4OH, as many milliliters as needed to fully soak the teflon basket. The solution in the beaker was heated to 75°C and 1 part H_2O_2 was added and then reheated to 75°C, and bubbles appeared. The sample basket was placed in the beaker for 10-15 min. Then the sample basket was rinsed in a large volume of DI-water. The residue of base piranha was discarded in a base waste container. The sample basket was rinsed with IPA and samples were taken out one by one and blown dry with nitrogen.

Functionalizing in solid state after cleaning

1-200mM of various dithiol-solutions (12EDT, 13BDT, 14BuDT, 14BDT, 18ODT) were prepared by adding dithiols to EtOH after which the mixture was placed under bath sonication for 15min. The gold nanowires - dropcast from suspension on a substrate (Si or glass sample holder) and cleaned in either a plasma cleaner (Section 3.4) or with base piranha (Section 3.4) to remove the PVP capping agents - were quickly placed in 4ml of 2-200mM dithiol in EtOH solution for 24-72h. After functionalization the samples were washed with EtOH, then placed in EtOH in order to redissolve the unattached dithiols, washed with EtOH again and placed in IPA for 30 seconds to remove EtOH. The samples were either used immediately or stored in a vial with EtOH.

Assembly with nanowires cleaned and functionalized in solid state

The substrates with functionalized nanowires were taken out of EtOH and washed with IPA, then blown dry with nitrogen. The substrates were wetted with octane and placed in a quantum dot in octane solution for times ranging from 5min-24h, for the quantum dots to attach to the nanowire surfaces. The substrates were then cleaned according to the '5 step cleaning process': substrates were taken immediately out from quantum dot solution and held in 15ml octane (1) to wash off the excess of quantum dots. Then they were transferred to a second vial with 15ml octane (2) and moved sturdy to remove any unbound quantum dot leftovers. The substrates were then kept in ACE (3) and IPA (4) for 30s, and blown dry with nitrogen (5) (see Figure 3.3). They were stored in a sample box in air.

Spincoat for Layer-by-Layer (LbL) method

To assembly multiple layers of quantum dots on substrate (either with or without nanowires), a Layer-by-Layer recipe was used as reported previously[42][43]. A substrate (either Si or glass) was placed in a spincoater (Polos spin150i) in a downflow cabinet and 5μl dithiol in ACN solution was dropcast (the '0th layer'). This was then soaked for 10 seconds and spincoated (20 seconds at 1000rpm). Then 5μl ACN was added and spincoated to remove unattached dithiols, and repeated a second time. Now the layering steps started. The first layer: 5μl quantum dot in octane solution was added and soaked for 10 seconds, then spincoated. 5μl dithiol in ACN solution was added for a ligand exchange, soaked for 10 seconds and spincoated. Then 5μl ACN was added and spincoated to remove unattached dithiols, which was repeated a second time. 5μl octane was dropcast and spincoated to remove unattached dots. For multiple layers the layering steps were repeated as many times as desired. After the spincoating, the samples were stored in a sample box in air, but preferably measured as soon as possible. We used a 25-30mg/ml quantum dot in octane solution, which resulted in 20nm for 1xLbL, and over 100nm for 3xLbL.

3.5 Scanning Electron Microscopy

Scanning electron microscopy (SEM) images were obtained with a FEI Verios 460 operating at 5kV and 100pA unless stated otherwise. An Everhart Thornley Detector (ETD) and Through the Lens Detector (TLD) were used to obtain the SEM images at working distances between 2-4mm. Samples were always kept in ACE and IPA for 30 seconds before SEM-imaging to prevent from carbon deposition. The best images were obtained using a TLD detector in immersion mode at a working distance of less than 2.5mm. For imaging of samples on glass substrate, the samples were covered with a conductive polymer (ESpacer-300, Showa Denko K.K.) which was connected to a metal sample holder via copper-tape to prevent from charging of the substrate. ESpacer was placed on the samples by the use of a spincoater for 45 seconds at 4000rpm or by dropcasting and blowing the excess off by a nitrogen gun. Then the samples were dried one minute in open air and placed on a hotplate at 90°C for 10 minutes. To wash off the ESpacer, the samples were held two times one minute in DI-water.

3.6 Focused Ion Beam

Focused Ion Beam (FIB) was used to obtain cross sections of samples at the nanoscale. A focused beam of gallium ions dissected the sample in a precise and controlled manner. A 500 nm layer of platinum was deposited in-situ prior to the ion beam exposure for obtaining a sharper cut. After tilting the substrate holder, images of the cross section were obtained with a FEI Helios Nanolab 600 microscope operating at 5kV and 100pA-0.5nA. Secondary electrons (SE) were obtained both with an ETD and TLD detector at 4mm working distance.

3.7 Atomic Force Microscopy

Atomic Force Microscopy (AFM) was done with a Veeco Dimension 3100 AFM, a high resolution scanning probe microscope with resolution on the order of sub nanometer. AFM was used to acquire the layer thickness of a quantum dot covered substrate. By the use of a metal tweezer a thin line of quantum dots was removed from the substrate, without damaging the substrate itself. A linescan was done over this line to find the difference on and off the quantum dot layeres.

3.8 Optical Characterization and Modeling

3.8.1 Photoluminescence (PL) measurements

To excite the samples in photoluminescence measurements, a 532 nm continuous wave laser (WITec, 40 μW) was focused through a 100X objective (0.9NA). Emission was collected through the same objective and fed to a fiber coupled spectrometer (Acton SP-2150i, Princeton Instruments). A long pass filter was used to ensure signal in the long wavelength range and block the reflection of the incoming beam. A calibration measurement was done to normalise the obtained spectra.

3.8.2 Absorption measurements using Integrating Sphere Microscopy

Glass sample holder

For the optical measurements, the assembly of the nanowires with quantum dots was done according to the method described in Section 3.3, but on a glass substrate that was marked by the use of a diamond cutter. Since the glass sample substrates (made from microscope glass slides, 65x7.9x1.5mm) were too thin for the sample holder on the 3D Piezo Stage, the bottom part of the glass was cut off and the glass sample was mounted to a thicker piece of glass by the use of transparent nailpolish, held together by a clip and dried for 30-60min (see Figure 3.4).

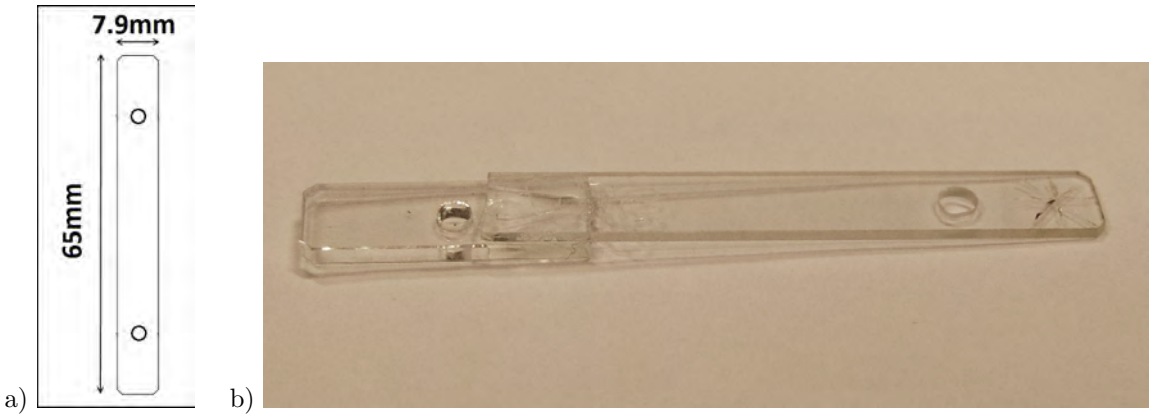

Figure 3.4: **Glass sample holder as used for the optical measurements.** Right: bottom part of the holder was cut off and mounted to a thicker piece of glass in order to prevent drifting of the sample in the sample holder.

Optical setup

The absorption measurements were conducted with a home-built optical setup. The optical measurements were based on the exact measurement of both the reflection off the sample, the scattering from the sample and transmission through the sample simultaneously, to extract the absorption in the sample (the absorptance) (see Figure 3.5 for the set-up).

The sample was mounted on a sample holder on a 3-axis piezoelectric stage (Piezosystem Jena Tritor 400 CAP) and placed inside an integrating sphere (IS, a custom modification to a GPS-020-SL standard integrating sphere built by LabSphere) which itself was positioned on a mechanical stage allowing it to be moved up and down to accomodate loading the sample. The sample was inserted into the IS through a narrow slit to minimize light loss. An ultra-long working distance microscope objective (Miutoyo M Apo Plan NIR 50x NA 0.42 objective, 17mm WD) was positioned accurately to the IS. The long working distance of the objective was required to illuminate single nanostructures. A supercontinuum laser (Fianium WL-SC-400-4) was sent through an acousto-optical tunable filter (Fianium AOTF, Crystal Technologies) with a wavelength range between 400-1100nm. A tightly focused beam was used to illuminate the structure and the incoming light power was on the order of several μW, depending on the wavelength used. Three photodetectors (Thorlabs amplified Si detectors, PDA100A) were used to detect (1) Reflection (2) and Transmission/Scattering, and (3) to correct for fluctuations in the laserpower. Photodetectors were connected to Stanford Research System SR830 lock-in amplifiers. A mirror (Thorlabs PF10-03-P01) was used for a Reflection reference measurement. A $\lambda/2$ plate allowed for measuring different polarizations, and a CCD Camera combined with a white light source allowed for navigating to the desired nanostructure on the sample.

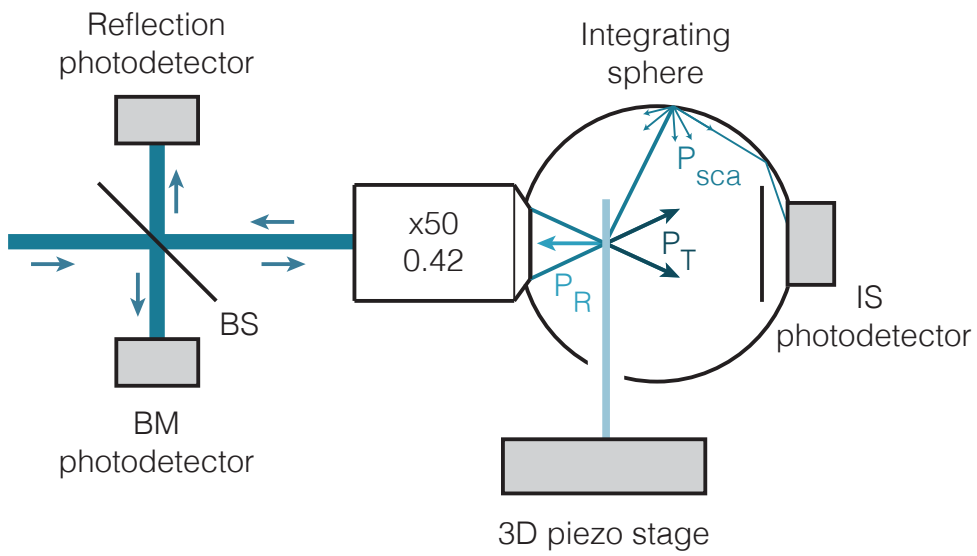

Figure 3.5: **Schematic of the optical setup used for absorption measurements on single nanostructures.** By the use of an ultra-long working distance microscope objective, laserlight (400-1100nm) is focused on a sample that can be moved on the nanoscale. In an integrating sphere both the scattered (P_{sca}) and transmitted (P_T) power are detected. Combining these values with the reflected (P_R) power, the absorptance can be substracted. A beam splitter (BS) is used to guide the light, and the a beam monitor (BM) is used to detect and correct for fluctuations in laser power at different wavelengths ([44] (*Image of the optical setup was used by permission of S. Mann*).

Data analysis

The absorptance A in the nanoscale samples measured by the integrating sphere microscopy setup was calculated as follows:

$$A = 1 - \frac{R_m}{R_r} - \frac{ISm}{ISr} - C \tag{3.1}$$

with R_m the measured reflection and R_r the reference reflection measurement, IS_m the measured scattering in the integrating sphere and IS_r the reference transmission measurement R_r is measured by placing a silver mirror in the focal plane of the objective, and IS_r by sending the focused beam through a hole in the sample, or by placing no sample in the IS. The constant C was included to correct for any losses such as the laser hitting the second interface of the sample (the back), which will not be detected and is assumed to be constant and in the order of 4% (0.04, the reflection from glass). From this energy balance we find a percentage for the absorptance in the sample after illumination.

3.8.3 Theoretical modeling

To predict the behaviour of a gold nanowire covered with PbS quantum dots, Mie Theory was used. This theory has been introduced in Section 2.4.1 and can be used to model the absorption cross section C_{abs} and electric field density $|E|^2$ in nanowires. We used a model written by Sander Mann which to predict SPRs and electric field densities in metal-semiconductor core-shell nanowires[4]. This code was used to compute the Mie coefficients for an infinitely long cylinder. Since an infinitely long cylinder is not spherically symmetric, the polarization of the incoming plane wave is of importance in understanding the resonances that can occur, as mentioned in Section 2.3. Therefore we distinguish the TE or TM polarization of the absorption cross section. Also, since the cylinder has an orientation, we distinguish a resonating propagation going clockwise or counterclockwise, resulting in the following expression for the absorption cross section in TE (similar for TM)[4]:

$$C_{abs}^{\mathrm{TE}} = C_{abs,m=0}^{\mathrm{TE}} + 2\sum_{m=1}^{\infty} C_{abs,m}^{\mathrm{TE}} \tag{3.2}$$

where m is the number of angular nodes in the field distribution, which must be accounted for twice when $m \geq 1$ (clockwise and counterclockwise). By dividing the C_{abs} by the actual size of the nanoparticle - the geometrical cross section C_{geo} - we can calculate the absorption efficiency η_{abs}.

From absorption cross section to absorptance

Since we measure absorptance A (fraction of the light being absorbed) and the Mie Theory used for this project shows results in terms of absorption cross section C_{abs}, we need to convert one to the other in order to compare theory with experiments. In the same way as described by Mann et al[44], we assume a Gaussian profile of the laser beam. Using the beam radius at its narrowest spot $\omega_0 = \frac{\lambda}{\pi NA_{eff}}$ with λ the wavelenght of the incoming (laser) light and the numerical aperture NA_{eff} we find as a conversion between absorptance A and absorption cross section C_{abs}:

$$A = C_{abs}\sqrt{\frac{2}{\pi\omega_0^2}} = C_{abs}\sqrt{\frac{2\pi \mathrm{NA}_{eff}^2}{\lambda^2}} \tag{3.3}$$

Absorptance: Beer-Lambert Law

The Beer-Lambert Law was used to get insight into the absorption in a quantum dot layered film. We used:

$$A = 1 - e^{-kz} \tag{3.4}$$

$$k = \frac{4\pi K}{\lambda} \tag{3.5}$$

with K the imaginary part of the refractive index of the quantum dots, obtained by ellipsometry measurements.

3.8.4 Data processing

Theoretical modeling was done by the use of Mathematica 10.0, data processing of optical measurements was done by the use of Matlab R2014b. Witec Project FOUR was used to analyse PL-spectra.

Chapter 4

Chemical Synthesis of Hybrid Nanostructure

In this Chapter the results of the chemical syntheses of quantum dots and nanowires are shown. Details on both the failed and succeeded assembly of a quantum dot/nanowire hybrid nanostructure are discussed. The Layer-by-Layer method as explained in the previous Chapter was done to ensure high absorption signals in optical measurements.

4.1 PbS quantum dots

We synthesized PbS quantum dots with both the hot injection method and the cold injection method, as discussed in Section 3.1 and kept them in octane solution. The desired concentration could be prepared by dilution or evaporation of the obtained solution. We synthesized multiple batches of quantum dots, and three different batches were chosen for further research: two batches from the hot injection with relatively large size dots (small bandgap) which were easier to detect by SEM imaging, and one batch with the cold injection method that provided us with smaller quantum dots with a bandgap in the detectable range of the optical measurement equipment.

Figure 4.1 depicts a series of absorption spectra obtained by UV-Vis absorption measurements. The hight of the peaks is normalized. One batch (second curve in Figure 4.1) seems to show a double peak, implying that two apparent sizes are present in one batch. A Gaussian fit was done to find the (average) bandgap, and the standard deviation gives insight into the size distribution. The location of the maximum corresponds to the bandgap, at 910nm, 1573nm and 2026nm (1.36eV, 0.79eV and 0.61eV resp.). From the relation between PbS quantum dot size and bandgap - as introduced in Section 2.2.1 - the diameters are calculated at 2.95nm, 6.04nm and 9.5nm resp[16], and by using a FWHM of the fitted peak we find the size distribution to be ±25%.

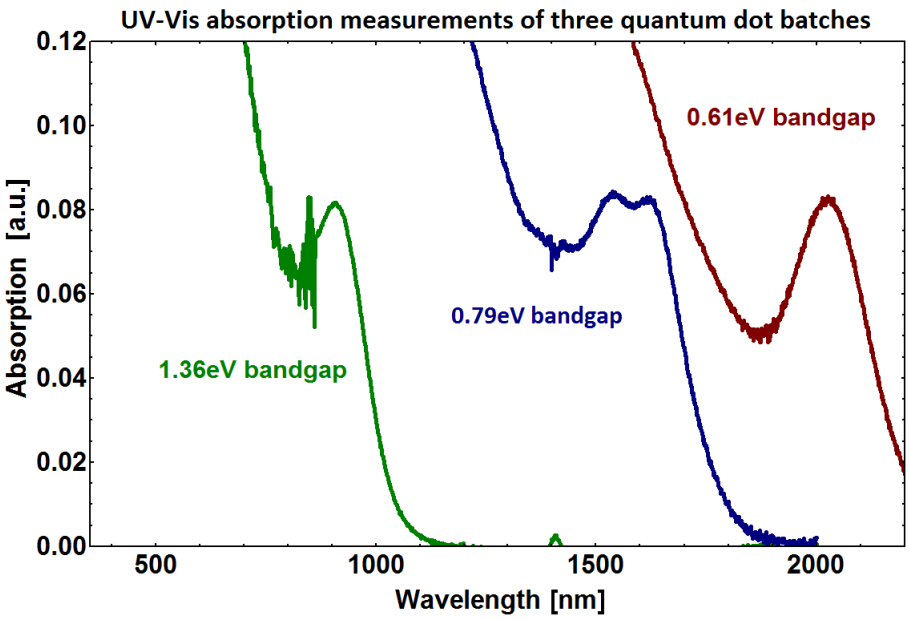

Figure 4.1: **UV-Vis absorption measurements of three quantum dot batches.** The maximum of the absorption peak corresponds to the bandgap of the quantum dots, at 910, 1573 and 2026nm (1.36eV, 0.79eV and 0.61eV resp.). The height of the peak is normalized and given in [a.u.].

4.2 Gold nanowires

Nanowire synthesis was performed with both 55.000 and 360.000 molecular weight (Mw) PVP as the reaction agent and nanowire capping agent (see Figure 4.2 (a) for the chemical formula of PVP). It was previously reported that for silver nanowire synthesis, using PVP with higher Mw resulted in better growth[45][46]. In our synthesis, the 55.000 Mw PVP led to clusters of nanowires during the washing steps, and the nanowires did not redisperse even after long sonication and shaking (see Figure 4.2 (b)). Using 360.000 Mw PVP, nanowires with diameters ranging between 80nm - 200nm capped with PVP were obtained in EtOH suspension, and the average nanowire diameter was around 100nm. The nanowire diameter size depends on the gold decahedron seeds, since larger decahedrons produce thicker nanowires[30] (see Figure 4.2 (c)). Lengths were in the range of tenths of microns although this changed over the course of the project since sonication broke the nanowires. Figure 4.3 (a) shows large triangular plates and self-seeded particles as byproducts of the synthesis. SEM imaging showed the pentagonal shape, as can be seen from the top in Figure 4.3) (b), which after FIB cross section imaging turned out to be less symmetric in cross section than expected as can be seen in Figure 4.15 at the end of this Chapter. This non-symmetric cross-section can be explained by the growing procedure of gold, which is more difficult than with for example silver nanowires. The gold nanowire synthesis leads often to geometric variations within one batch, explaining the large amount of byproducts like triangular plates and ribbon like wires.

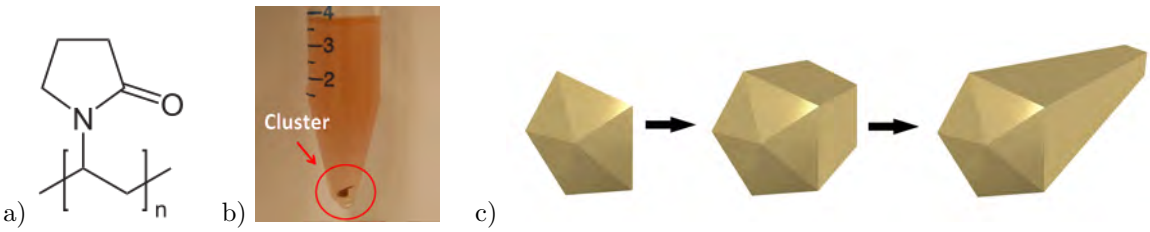

Figure 4.2: **(a) Repeating unit of Polyvinylpyrrolidone (PVP),** the nanowire reacting and capping agent. **(b) The use of 55.000 Mw PVP led to clustering of the nanowires**, even after washing. **(c) The growth mechanism of the nanowire synthesis.** Decahedron seeds were used, and PVP acted as the reaction agent.

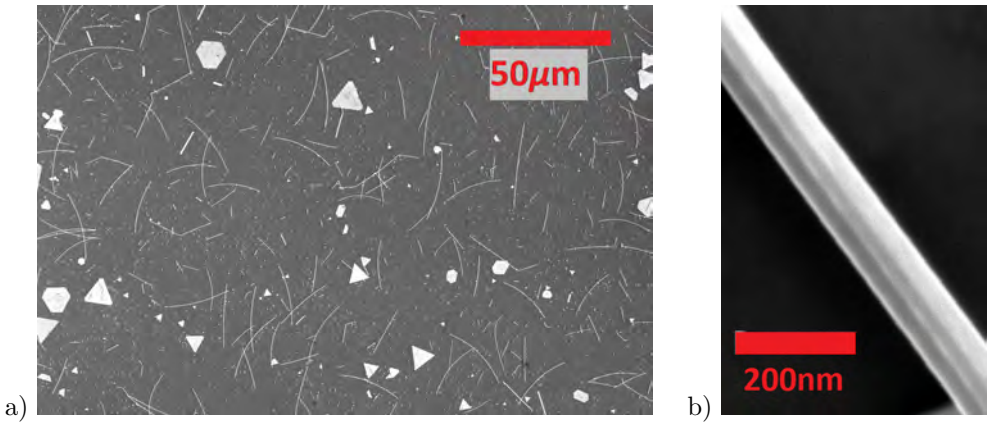

Figure 4.3: **(a) SEM imaging shows nanowires with diameters ranging between 80nm-200nm and lengths of tenths of microns.** Gold nanoparticles and triangular plates were byproducts of the synthesis. **(b) SEM imaging shows the sides of the pentagonal-shaped nanowire.**

4.3 Assembly of the quantum dot/nanowire hybrid nanostructure

Several approaches have been adopted to assemble the quantum dots on the surface of the nanowires, as mentioned in the previous Chapter (Section 3.3). In the next two Sections we distinguish between a failed and a successful assembly, with a removal of PVP as the difference. Dithiols were used as the linker molecules between the two nanostructures.

4.3.1 Quantum dot/nanowire hybrid nanostructure without PVP removal

Functionalize quantum dots

Quantum dots capped by oleic acid exchange ligands to dithiols when brought into their vicinity. This functionalization is driven by Pb-S bond formation and desorption of oleic acid, or by the dissociative adsorption of dithiols on the quantum dot surface which again results in desorption of oleic acid[14]. This is often done in solid state, but by adding an excess of dithiols to a quantum dot solution in octane we assume that the quantum dots should theoretically become functionalized with dithiols without cross-link effects. Our solution with quantum dots functionalized in dithiols in octane looked transparent with a slight brownish shade, implying that there were no or few clusters. After the addition of both functionalized and non-functionalized nanowires in solution, the solution stayed transparent, but SEM imaging showed clustering in all cases. It seemed that the functionalization of quantum dots did not work, and/or that the cross-link effect appeared.

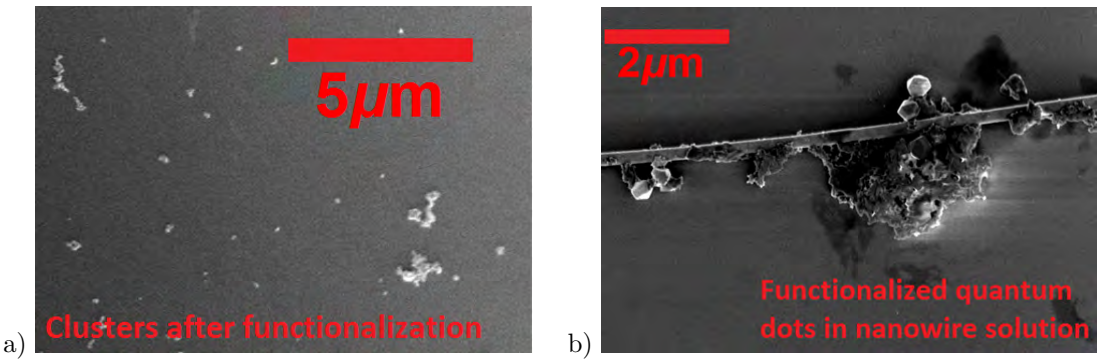

Figure 4.4: **SEM images of samples with functionalized quantum dots.** (a) Quantum dots functionalized in solution and dropcast on Si. We see clusters. (b) When functionalized nanowires (14BDT) in solution were added to the functionalized quantum dot solution, the quantum dot clusters seem to precipitate onto the nanowires.

Heating in quantum dot solution

The nanowires that were dropcast from solution on a Si substrate and then kept in a dithiol solution for 24h, were placed in a 25mg/ml quantum dots in octane solution. The solution was then heated to 100°C for 24h with the objective to help drive the chemical attachment and expedite the quantum dot assembly on the nanowire surface. SEM images show remarkable results: the quantum dots formed nanorods, as can be seen in Figure 4.5 (a). A similar self assembly is reported before by Vanmaekelbergh et al. [47]. In this formation ligands come off the surface. Also, the 'nanorods' seem to repell the nanowires as is seen in Figure 4.5 (b). A distance of several hundreds of nanometers is clear of quantum dots. This repulsion could be due to the PVP still capping the nanowires, but this phenomenon was not further researched.

Dipping (functionalized) nanowires in quantum dot solution

We also functionalized nanowires in dithiol solution without dropcasting on a substrate first. Nanowires that were either functionalized or non-functionalized in solution were dropcast on Si substrates and dipped into a quantum dot solution for 10 seconds. Some samples were dipped into a dithiol solution

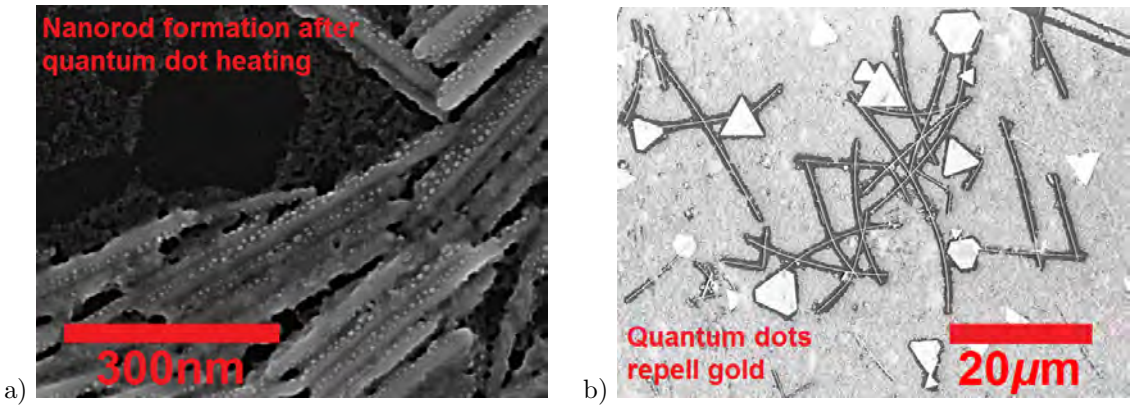

Figure 4.5: **SEM images of formation of nanorods after heating substrates with nanowires in quantum dot solution.** The quantum dots formed into nanorods (a), and repelled the gold nanostructures (b).

first. Quantum dots covered the nanowires, regardless whether the nanowires were functionalized or not, and regardless whether we started with dithiol dipping or not. Since the quantum dots covered the substrate in a similar fashion, we assumed that the quantum dots had no preferrence to the nanowires.

Soaking (functionalized) nanowires in quantum dot solution for longer times

Also no difference was found between functionalized-in-solution and non-functionalized nanowires, dropcast on a substrate and brought in contact with quantum dots by either dropcasting quantum dots on the substrate or placing the substrates in a quantum dot solution. Figure 4.6 shows SEM images of nanowires functionalized in solution and non-functionalized nanowires, placed in a 25mg/ml PbS quantum dot (0.61eV) in octane solution for 20h or vertically dipped in a similar quantum dot solution to soak the sample for 1 minute. Quantum dot clusters are found both on the nanowire and on the substrate, and the quantum dots on the substrate seemed to avoid the nanowire. We attribute this to the drying of quantum dots on the substrate. No conclusions about assembly times were drawn from these experiments.

The assembly did not seem to succeed and the problem could be either the attachment of dithiols to the nanowires during functionalization, or the attachment of quantum dots to the functionalized gold nanowires. To check the first assumption, gold nanoparticles of around 10nm diameter were added to both functionalized in solution and non-functionalized gold nanowires. Since gold has a high binding affinity to the -SH group of the dithiol, this experiment could give us insight in the success of the functionalization. In both cases the gold particles attached to the nanowire surfaces with the same moderate affinity, although it was expected that a succesful functionalization would result in a very high affinity of gold nanoparticles to the nanowire surface. From this we conclude that the functionalization of nanowires could be the problem.

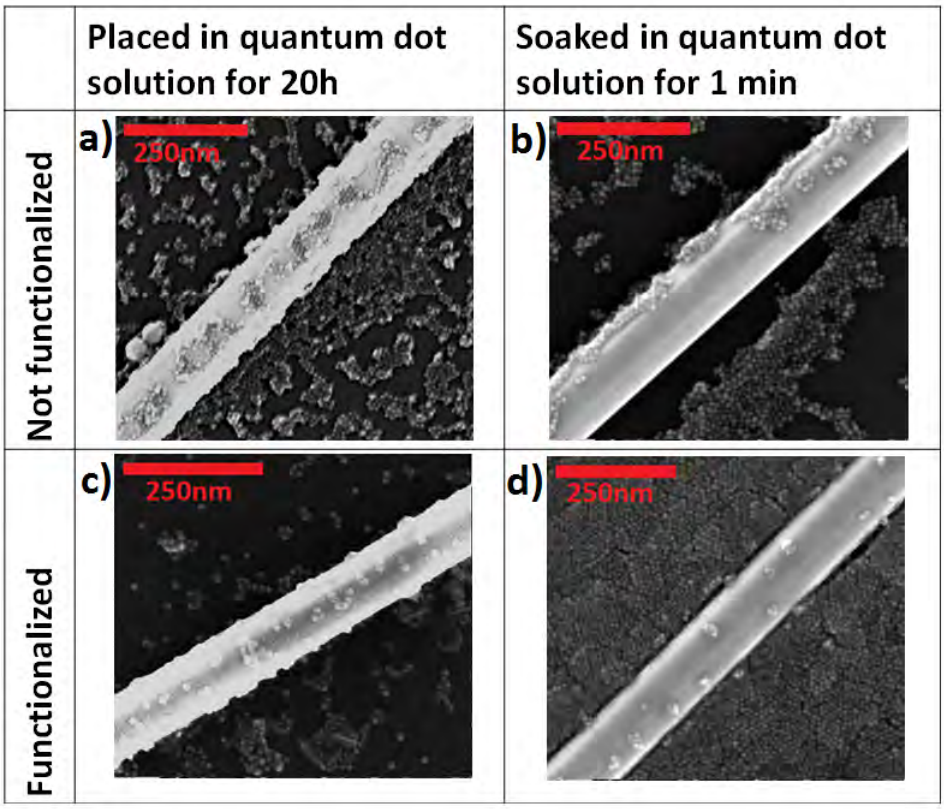

Figure 4.6: **SEM images to compare nanowires with and without functionalization, dropcast on substrates and placed in a quantum dot solution.** (a) and (b) were not functionalized, (c) and (d) were functionalized in solution with 14BZDT. The substrates (a) and (c) were put in a 25mg/ml PbS quantum dot solution (0.61eV bandgap) for 20h. (b) and (d) were dipped in a similar quantum dot solution for 1 minute.

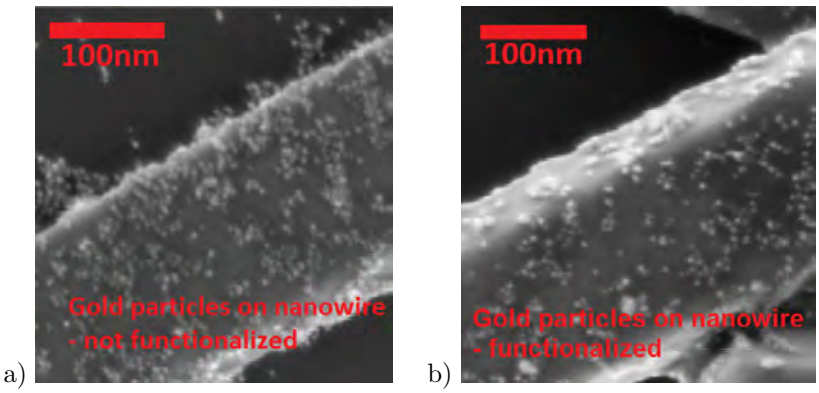

Figure 4.7: **SEM images of gold nanoparticles brought in contact with non-functionalized (a) and functionalized (b) nanowires**. Both images are alike, implying that the functionalization did not change the nanowire surface.

4.3.2 Quantum dot/nanowire hybrid nanostructure with PVP removal

From the previous results we assumed that the functionalization of the nanowires failed, presumably because the PVP chains were too long and dense for the short dithiols to penetrate through to the nanowire surface. A new approach was taken: cleaning the nanowires to assure the removal of the PVP by plasma cleaning or base piranha cleaning. The method of this assembly was discussed in more detail in the previous Chapter (3.3) and is illustrated in Figure 4.8. After assembly we performed the '5 step cleaning process', which appeared to be essential to remove quantum dots from the substrate. SEM imaging showed a clear preference of the quantum dots to the nanowire surfaces implying that the PVP removal step was crucial in the attachment of quantum dots to the nanowires. Figure 4.9 shows the nanowires covered with quantum dots.

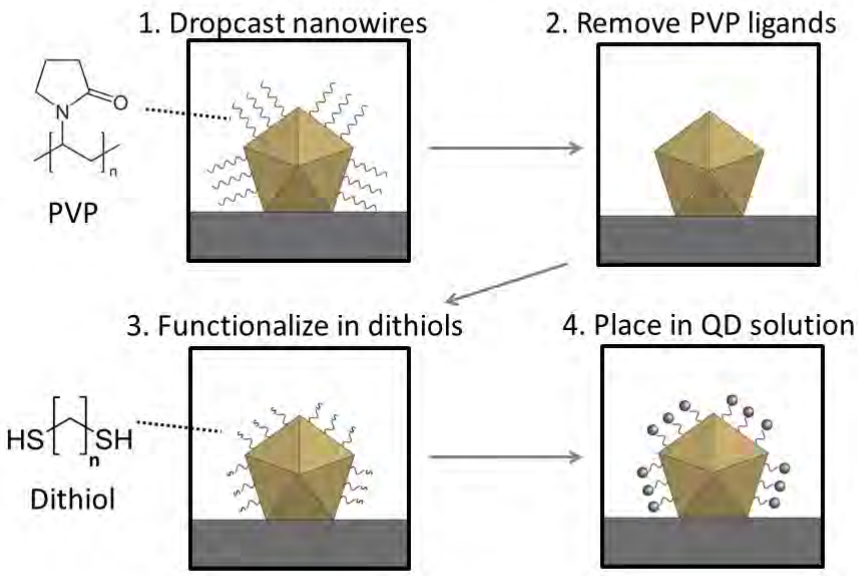

Figure 4.8: **The assembly of quantum dots to nanowires by the use of an intermediate cleaning step.** Gold nanowires were dropcast from suspension on a substrate (Si or glass). The PVP-capped gold nanowires on substrate were cleaned in either a plasma cleaner for some minutes or with 'base piranha', then the substrate was put in a dithiol in EtOH solution immediately for the dithiols to form a SAM on the gold nanowire surface. After functionalization the substrate was put in quantum dot in octane solution. The substrates were then cleaned according to the '5 step cleaning process'.

Plasma cleaning

1, 3, 5 and 10 minutes of plasma cleaning was tried in order to find whether the time of plasma cleaning was of influence for the PVP removal and quantum dot attachment. We could not find a clear correlation between the time of plasma cleaning and the quantum dot coverage. 1 minute showed coverage, although in some cases after 3 minutes plasma cleaning better stacking of quantum dots was visible (as in Figure 4.9 (a) compared to (b)). SEM images of the 5 and 10 minutes plasma cleaned nanowires showed dark spots on the surface, and it looked like they were surrounded by little bright spots (see Figure 4.10). This might mean that atoms were sputtered off the gold surface and the nanowires were damaged during longer plasma etching times, although gold should stay unaffected by oxygen plasma. For the remaining work we pursued with 3 minute plasma cleaning. Base piranha was tried as cleaning procedure to test the succes of plasma cleaning procedure, as discussed in Section 4.3.2.

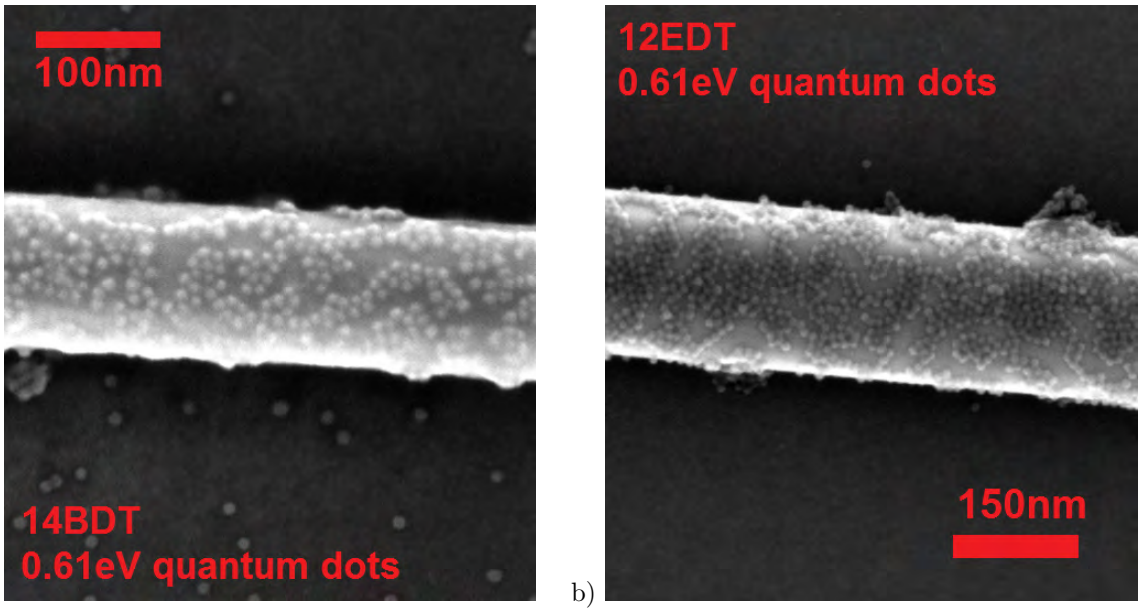

a) b)

Figure 4.9: **SEM images of nanowires (plasma cleaned before functionalization) assembled with quantum dots.** (a) 1 minute plasma cleaned and functionalized with 14BDT and (b) 3 minutes plasma cleaned and functionalized with 12EDT. Both were placed for 60min in a 0.61eV quantum dot solution (25mg/ml in octane). This showed a quantum dot coverage of around 50%. After the '5 step cleaning process' the substrate is free from quantum dots.

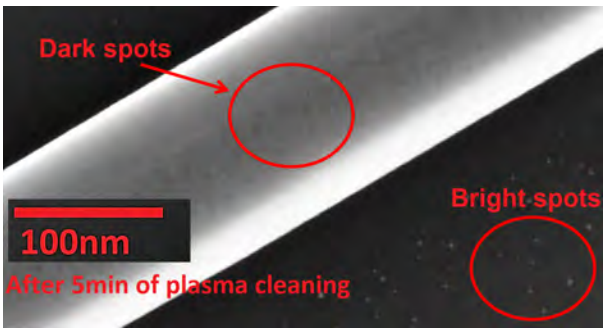

Figure 4.10: **SEM image of gold nanowire dropcast on Si substrate and plasma-cleaned for 5 minutes.** Little bright spots surrounding the nanoparticles and 'dark holes' are visible.

Dithiol molarity and time of functionalization

After plasma cleaning the substrates were put in dithiol solutions of varying concentrations and functionalized for 24-72h. For a 1mM or 4mM dithiol solution, not all the nanowires on the sample substrate were covered in a similar fashion, but increasing the dithiol solution up to 200mM (20mM seemed to be sufficient but higher solutions were used to be sure) showed a uniform coverage of nanowires by quantum dots all over the sample. Since it seemed implausible that the amount of dithiols were the limitation, we performed a quick calculation to validate this assumption. SAMS form on gold with $4.5 * 10^{14}$ molecules/cm^2 [36]. With 2ml of 200mM dithiols we offer over 10^{20} dithiol molecules to the substrate, which is about 1cm^2 and not fully covered by gold. Extremely long functionalization times up to weeks were tried but did not show an increase in quantum dot on nanowire attachment.

Quantum dot concentration and time of assembly

25mg/ml quantum dot concentration gave better quantum dot coverage than 10mg/ml, but increasing up to 120mg/ml concentrations did not seem to improve the coverage further. 45-60minutes of assembly (substrate with functionalized nanowires in quantum dot solution) showed better coverage than 5 minutes, although these differences were not always clearly apparent. Longer assembly times sometimes exhibited worse coverage. Re-usage of a quantum dot solution yielded in poorer attachment and cluster formation. We assume that during the assembly an interaction between the substrate with nanowires and the quantum dot solution takes place, either from solvents on the substrate or dithiol/OA exchange, resulting in worse coverage of the nanowire and contamination of the quantum dot solution. Also we assume that ligand exchange could have caused the quantum dots to dissolve back into the octane. Using 'fresh' quantum dot solutions led to the best results.

Dithiols and quantum dot size

When comparing various ligands, SEM imaging suggested that 12EDT and 18ODT led to better coverage than 14BuDT. The combination of 9.5nm quantum dots with 12EDT sometimes seemed to produce better stacking, whereas the combination of 18ODT with the 6nm dots showed better coverage. Because the resolution during SEM imaging was not good enough to individually image the 2.95nm quantum dots, we could not find a relation between dithiols and nanowire coverage of these quantum dots.

Base piranha

The hybrid nanostructure made from nanowires that were cleaned by plasma etching showed uncovered spots on the nanowire surface (as is seen in Figure 4.9), indicating that either some PVP was still present, that the dithiols did not form a homogeneous SAM or that the quantum dots did not attach to every available -SH group. To support that the PVP removal by plasma cleaning was not the problem, base piranha cleaning was tried instead. This aggressive chemical solution oxidizes and dissolves organics. After the base piranha cleaning the procedure for assembly was done as depicted in Figure 4.8. SEM imaging showed a similar coverage of the nanowires, suggesting that the assembly was not hindered by PVP remainders (see Figure 4.11). We detected a significant reduction in numbers of nanowires on the substrate, suggesting that nanowires were wiped off the substrate into the base piranha solution. This could be explained by the 360° PVP-capping of the nanowires (also in between the substrate and the nanowire), which after cleaning lifted the nanowires off the substrate. This was further supported by colored spots on the substrate indicating removed nanowires.

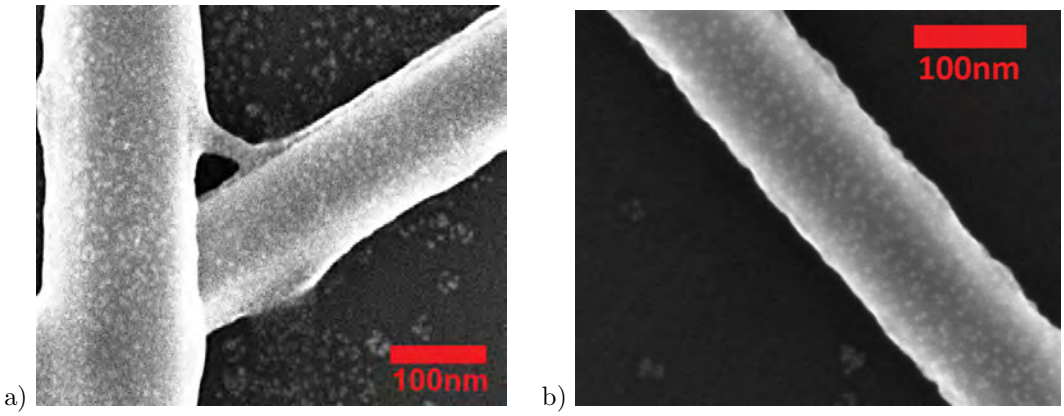

Figure 4.11: **SEM images of nanowires cleaned with base piranha before functionalization.** Functionalized with 12EDT (a) and 14BuDT (b). All were assembled with 25mg/ml 0.79eV quantum dots and showed a sub-monolayer quantum dot coverage, just as with the plasma-etched samples. (a) shows nanowires and quantum dots covered with something, presumably originating from the base piranha cleaning.

Second functionalization, second time in quantum dots

Nanowires covered with a sub-monolayer of quantum dots were functionalized in solution again, and put in quantum dots a second time to produce multiple quantum dot layers. SEM imaging showed accumulation of quantum dots on the substrate, suggesting that quantum dots were functionalized (ie the oleic acid was replaced by dithiols) and new quantum dots attached, but the attachment of new quantum dots to the sub-monolayer of quantum dots on the nanowires was not obvious and only happened at some of the sites. We did not observe better coverage of the nanowire surface after this second functionalization.

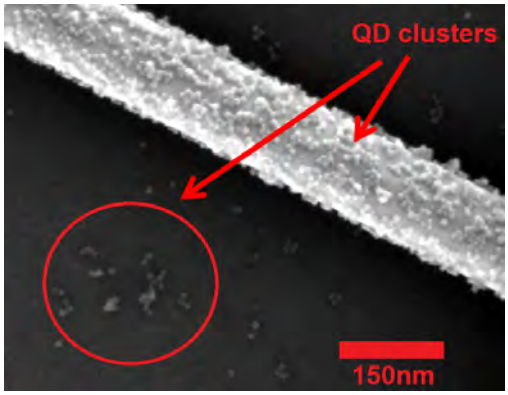

Figure 4.12: **SEM image of nanowire (from Figure 4.9 (b)) functionalized and placed in quantum dot solution a second time.** Clusterformation of quantum dots on the nanowire as depicted by the red arrow and on the substrate as seen in the red circle imply that individual dots were functionalized as well, and new dots attached in a second assembly. Empty spots are still present on the nanowire surface.

Layer-by-Layer (LbL) method for thick quantum dot layers on nanowires

To make homogeneous and thick layers of quantum dots on the nanowires, the LbL method was used as described in Section 3.3 in the previous Chapter. Spincoating 25mg/ml quantum dots with 200mM dithiol in acetonitrile solution showed uniform layers of quantum dots. We refer to a '1xLbL' spincoating when one layer of quantum dots and dithiols are spincoated on the sample, and '3xLbL' when this is done three times. Cracks in the quantum dot film indicate a succesful replacement of oleic acid, since the ligand exchange to shorter dithiols moves the quantum dots closer together causing the film to crack as can be seen in Figure 4.13. Figure 4.14 shows a cartoon of the method of Layer-by-Layer spincoating.

a) 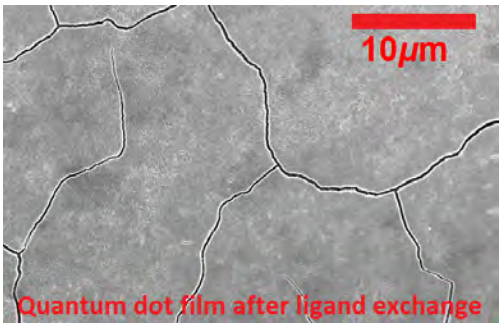

b) 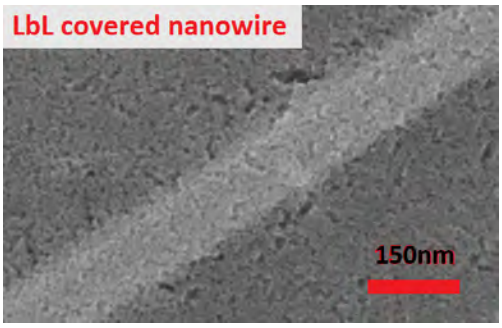

Figure 4.13: **(a) Quantum dot layers with the LbL method on a plain substrate.** Cracks in the quantum dot film indicate a succesful replacement of oleic acid by dithiols. **(b) Quantum dots assembled LbL on nanowires (b).** The nanowire is fully covered by quantum dots.

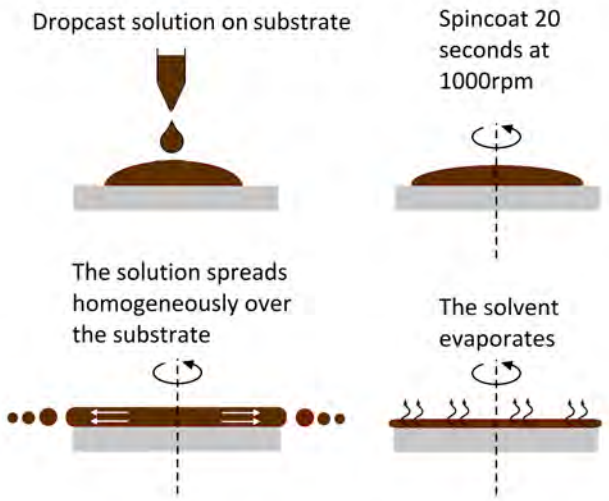

Figure 4.14: **Layer-by-Layer (LbL) method by the use of a spincoater.** Quantum dots and dithiols both in solution are spincoated layer-by-layer on either a Si substrate or a glass substrate with plasma-cleaned and functionalized nanowires covered with a sub-monolayer of quantum dots.

4.4 Focused Ion Beam imaging and Atomic Force Microscopy

Figure 4.15 shows cross sections of nanowires covered with quantum dots, obtained by Focused Ion Beam imaging, to gain insight into the quantum dot layer thickness after the LbL spincoating. We performed FIB both on Si substrates and glass substrates. We looked at samples with 1xLbL and 3xLbL on plasma cleaned and 12EDT functionalized nanowires, and 3xLbL on nanowires that were not cleaned and not functionalized. The resolution was not detailed enough to show differences in the nanowire-quantum dot interfaces with and without PVP removal, if any. The first thing we noticed is the shape of the nanowire, which was flatter than the symmetric pentagonal shape we expected (see Figure 4.15 (a)). It is possible that the gold nanowire synthesis led to geometric variations, although it is also probable that the view angle in FIB imaging caused the nanowire cross section to appear flat. By doing a tilt correction, we obtained images of cross sections as depicted in Figures 4.15 (b) and (c). The quantum dot layer on the nanowire was thinner than next to the nanowire. Also, on the right of the nanowire no quantum dots were apparent, presumably because the cracking in the film happened exactly next to the nanowire. We did not see this for every nanowire, so it is likely that most nanowires were fully covered. Looking at the 3xLbL samples as depicted in Figures 4.15 (b) and (c), it seemed that the more layers were spincoated on the sample, the smaller the difference between the thickness on and off the nanowire. The quantum dot coverage over the whole sample was not homogeneous and in the 3xLbL samples layer thicknesess could vary up to 40nm over hundreds of nanometers, as can be seen in Figure 4.15 (b) and (c). We do not attribute the difference in quantum dot layers in Figure 4.15 (b) and (c) to the nanowire treatment. In both samples we saw quantum dot layer thicknesses varying over the sample. The layers in the 3xLbL are thicker than expected, over 100nm. Again it should be noted that FIB imaging happens with a tilted sample holder which could misrepresent the size. To check this, AFM was performed on glass samples that were used for the optical measurements, to find the quantum dot film thickness. A small scratch was made on the substrate to remove the quantum dot film, and with AFM the difference between on and off the film was found. We found a 20nm - 30nm film thickness on 1xLbL spincoated samples and a 120nm - 150nm quantum dot film thickness on 3xLbL spincoated samples. Note that AFM only gives insight into the thickness of the quantum dot layers next to the nanowires, since AFM is a less precise technique and measurements on small nanostructures like the nanowires could not be performed.

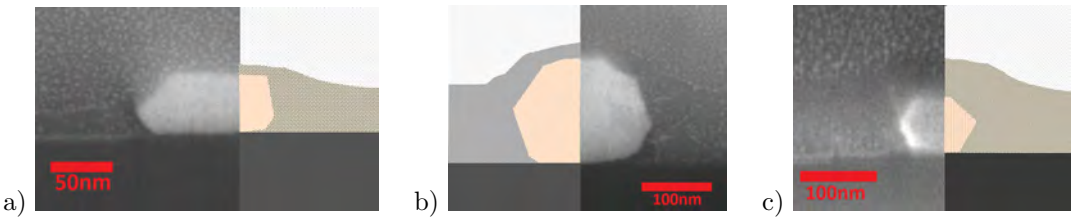

Figure 4.15: **FIB images showing cross-sections of three LbL samples with 12EDT dithiols and 1.36eV PbS quantum dots.** (a) 1xLbL on plasma cleaned and 12EDT functionalized nanowires, without tilt correction. (b) 3xLbL on plasma cleaned and 12EDT functionalized nanowires and (c) 3xLbL on nanowires that were not cleaned and not functionalized. (b) and (c) were obtained with tilt correction.

4.5 Summary

In this Chapter results of the quantum dot and nanowire assembly were shown. To assemble the two nanostructures, dithiols were used as linker molecules. From functionalization in solution it appeared that the nanowire capping agent PVP blocked the functionalization. Cleaning treatments removed PVP and aided a successful assembly. A nanowire coverage of at maximum 50% was seen, where no quantum dots were apparent on the substrate. Functionalizing and assembling these samples with quantum dots a second time did not result in multiple quantum dot layers. To assure enough absorption signal for optical measurement as will be discussed in the next Chapter, a Layer-by-Layer spincoating method was performed to fully cover the nanowires with quantum dots. Films of quantum dots were covering the nanowire, where the quantum dot layer thickness next to the nanowire was thicker than on the nanowire. In the next Chapter, these samples will be characterized optically.

Chapter 5

Optical Modeling and Characterization of the Hybrid Nanostructure

In the previous Chapter we discussed results of the hybrid nanostructure assembly. This chapter describes the modeling and optical characterizations of the assembled hybrid nanostructures obtained from the Layer-by-Layer method as explained in the previous Chapter. Results of the optical characterizations including absorption measurements, absorption mapping and photoluminescence are shown, compared with theory, and discussed.

5.1 Predictions from theoretical modeling

Mie Theory was used to predict the absorptance in nanowires with and without PbS quantum dot coverage. The dielectric functions for gold were obtained from the Handbook of Palik[35], the dielectric functions for PbS quantum dots were obtained from ellipsometry-measurements, as discussed in Section 3.1.

Plain uncovered gold nanowires support a resonance at 500nm in TE polarization, irrespective of their diameter. Addition of a quantum dot shell alters the dielectric of the surrounding medium and redshifts this resonance. The thicker the shell, the more the resonance shifts to the red. Figure 5.1 shows the modeled absorptance in 100nm diameter nanowires covered with a single layer of 1.25eV quantum dots, or multiple layers of quantum dots. This graph includes the absorptance in an uncovered nanowire for comparison. From this Figure it is seen that a thicker quantum dot layer results in more absorption and a redshifting resonance. A plain nanowire absorbs about 12% at 500nm resonance, which changes to 26% at 525nm for a 20nm thick shell, 28% at 560nm (30nm shell), 31% at 580nm (40nm shell) and 32% at 610nm (50nm shell). A single quantum dot layer introduces a shell of only a couple of nanometers thick resulting in an increase of absorption to 14%, where no clear resonance shift is seen. Since the dielectric function in the visible wavelength range is very similar for all three quantum dot batches, we expect the changes in resonance frequency to be mostly determined by shell thickness. In the (near) infrared range the absorption in both plain nanowires and the core-shell structure gradually decreases untill it reaches zero. Modeling of the electric field intensity $|E|^2$ for different shell thicknesses at resonance gives insight into the absorption enhancement. We see that the electric field is most strongly confined in the quantum dot shell, and increases with increasing shell thickness (see Figure 5.2). This suggests that the absorption enhancement stems from absorption in the quantum dot shell.

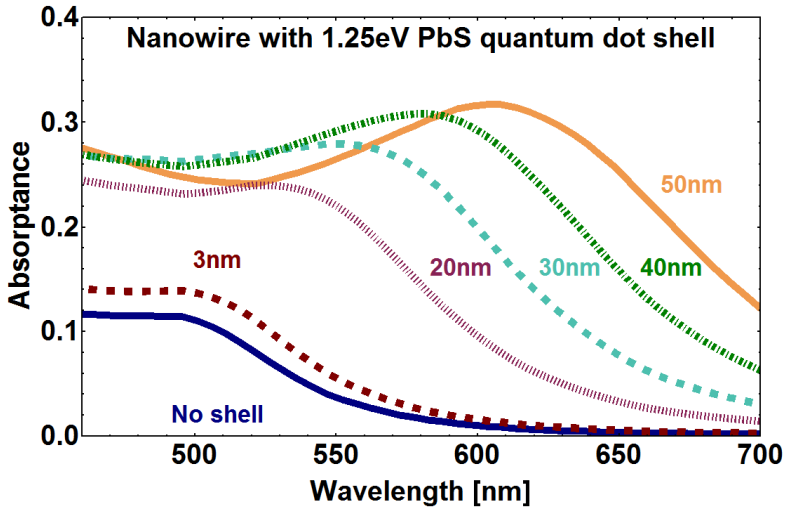

Figure 5.1: **Mie Theory modeling of absorption in TE polarization of 100nm gold nanowires covered with a homogeneous 1.25eV PbS quantum dot shell of different thickness.** Thicker quantum dot layers cause a redshift of the resonance.

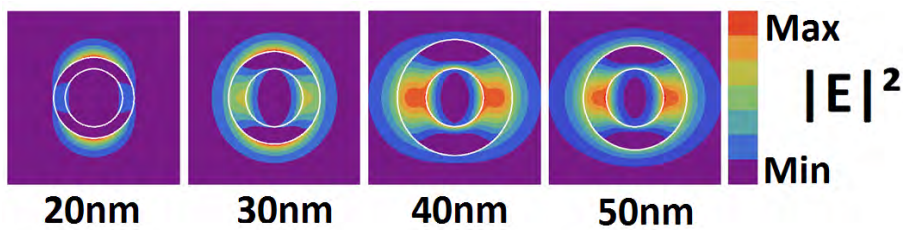

Figure 5.2: **Electric field intensities modeled with Mie Theory** in 100nm diameter nanowires with different shell thicknesses (20nm, 30nm, 40nm, 50nm) of 1.25eV quantum dots, at their resonance in TE polarization.

For comparison we modeled the absoption in uncovered nanowires with different diameter. We found that a change in uncovered nanowire diameter from 50-150 nm results in an absorptance change from 3-20% as can be seen in Figure 5.3. Bigger nanowires absorb more, but the resonance remains at 500nm.

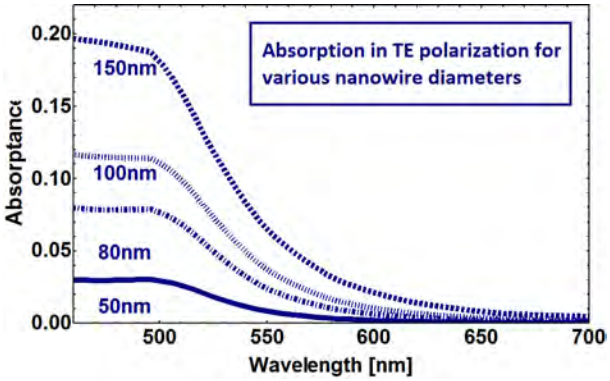

Figure 5.3: **Absorption in uncovered nanowires of different diameter.** Modeled by the use of Mie Theory.

5.2 Absorption measurements using Integrating Sphere Spectroscopy

Based on modeling our focus was on the visible wavelength range, but we also measured samples with 1.36eV quantum dots in the near-infrared because their bandgap was in the detectable range of our setup (up to 1100nm). We expect an increase in the absorption in the hybrid nanostructure together with a redshift of resonance in TE polarization when increasing the quantum dot layer thickness on the nanowire. We used the optics setup as described in the Method Chapter to measure absorption of single nanostructures. The ultra-long working distance microscope objective can focus the laser tightly with a power in the order of μW to scan over a single hybrid nanostructure. The spotsize of the beam has a radius of 1 μm. This gives a power of over 1000 suns (1sun=1kW/m^2) when focused on the sample. We sometimes noticed a slight color change after the measurement, implying that the high power damaged the sample. Therefore the electronic properties of the structure could have been damaged during the scanning, which must be taken into account in further research. A linescan of 3μm perpendicular to the nanowire long axis was performed to scan both on and off the wire, as is depicted in Figure 5.4 (a). By changing the polarizer 90° both the TE and TM modes of the NW were measured. In Figure 5.4 (b) both modeled and measured absorption in plain (uncovered) nanowires are displayed. This Figure shows a measured nanowire resonance in TE at around 500nm, which is supported by theory. The absorptance is around 12% in the model and higher in the measurement. This difference could be explained by a difference in nanowire diameter between model and sample. Also theory was based on a perfectly round nanowire diameter whereas our synthesized nanowires show a pentagonal non-symmetric cross section.

Preferably we would measure the absorption in the same nanowire both before and after coverage with quantum dots. Markers on the sample facilitate the selection of specific nanowires. Unfortunately the procedure to assemble the quantum dots on the nanowire often caused the nanowires to shift or sometimes even disappear, which made it very hard or impossible to find the exact same nanowire back on the sample. Hence no comparison could be made between nanowires before and after assembly. Most of the nanowires had a 100nm diameter and we used this size as an example for modeling, and used multiple measurements on uncovered nanowires for comparison.

Sub-monolayer coverage

The measurement of plasma cleaned nanowires covered with a sub-monolayer of quantum dots (as for example depicted in Figure 4.9) did not show a clear increase in absorption compared to plain nanowires. In the previous Sections we discussed the modeled absorptance in a nanowire covered with a single quantum dot layer, showing no resonance shift and only a slight increase in absorption (Figure 5.1). Any

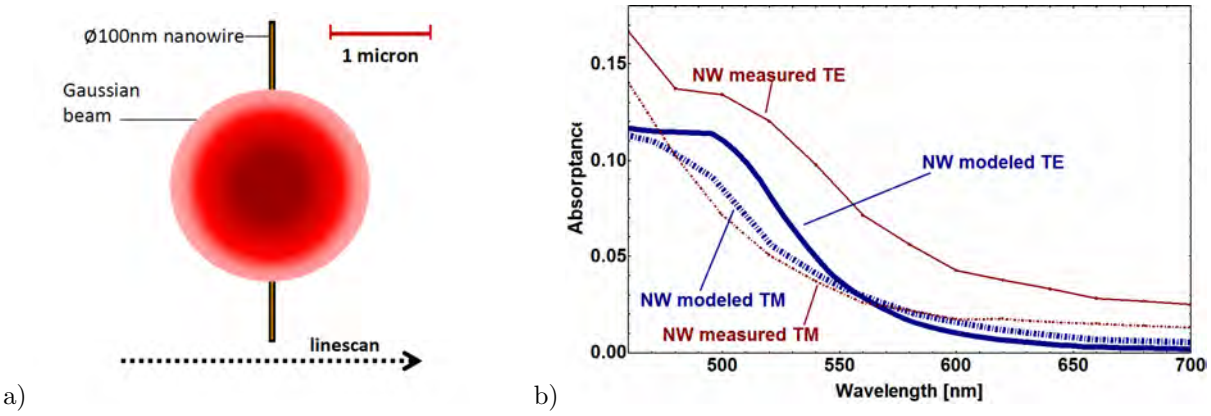

Figure 5.4: **(a) Cartoon of the laserscan over the nanowire.** The center of the Gaussian beam scans 3μm over the nanowire. **(b) Measured and modeled absorptance in uncovered gold nanowires of 100nm, both in TE and TM.** Measured nanowire (red lines with markers) shows a resonance at around 500nm, which is supported by theory.

minimal change measured in absorption could also come from variations in nanowire diameter, as is seen in Figure 5.4, so we continued absorption measurements on samples with thick quantum dot layers where we do expect a shift in resonance and an intensified absorption increase.

LbL fully covered nanowires

For the LbL samples the quantum dots not only cover the nanowire but the whole substrate. AFM measurements showed a 20nm-30nm quantum dot layer thickness (next to the nanowires) in samples that were spincoated once (1xLbL) and a 100nm-150nm quantum dot layer thickness (next to the nanowires) in samples that were spincoated three times (3xLbL). FIB showed that the quantum dot layer thickness on the nanowires is thinner than next to the nanowire, and this thickness can vary from nanowire to nanowire (FIB images are found in the previous Chapter). Because the beamspot of the laser is bigger than the nanostructure (diameter of 2μm), the measured signal also comes from quantum dots surrounding the nanowire. Thus the signal coming from the nanowire will be underestimated as we always measure both quantum dots and the quantum dot covered nanowire. Therefore we need to analyze the data carefully to distinguish between the absorption in the hybrid nanostructure and the absorption in the surrounding quantum dots.

A linescan of 3μm perpendicular to the nanowire long axis was done to measure the signal coming from the nanowire, in the desired wavelength range. This was repeated 10 times over 11μm in focal depth to find the exact point of focus. A density plot of the 3μm linescan - 11μm in focal depth - at 620nm shows the Gaussian profile of the beam as seen in Figure 5.5 (a). The highest intensity corresponds to the signal when exactly in focus on the covered nanowire. This signal was used to further analyse the absorption. Once we are in focal depth, we can also do spatial mapping of the nanostructures at a specific wavelength. Figure 5.5 (b) depicts an absorption map on a nanowire covered with a thick quantum dot layer. The image is taken at 525nm, which is off resonance. Here we can see that the absorption in the nanowire is 54% where it is 48% in the surrounding quantum dots. So also in the area off resonance the absorption is higher in the hybrid nanostructure than in the nearby quantum dot film, even though the quantum dot layer on the nanowire is probably thinner than next to the nanowire. Since in the LbL samples the nanowires were fully surrounded by quantum dots, the measured absorption was different from the modeled spectra which were based on a core-shell structure surrounded by air. Figure 5.6 displays the measured absorption in a nanowire covered with 20nm-30nm (1xLbL, (a)) and 120-150nm (3xLbL, (b)) spincoated 1.36eV quantum dots compared to the absorption of the quantum dot film in the near vicinity of the nanowire. The quantum dot layer on the nanowire was most likely thinner. The laser was polarized both perpendicular (TE) and parallel (TM) to the nanowire long axis, but only the TE polarization showed resonances, as expected. At every wavelength the hybrid nanostructure absorbs more than the quantum dot film alone. We divide the nanowire signal by the quantum dot signal. Now a clear peak arises at 550nm (a) and 650nm (b), as can be seen in Figure 5.6, which could depict the

redshifted resonance.

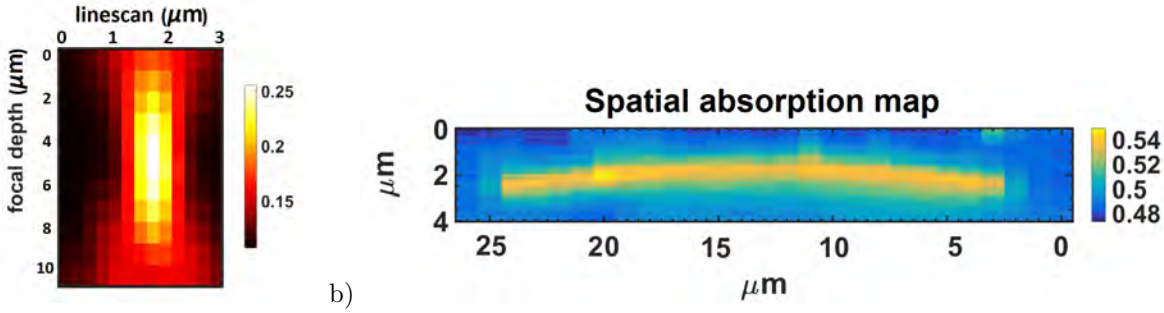

Figure 5.5: **(a) Density plot of the beamfocus** of the laserscan over the nanowire (x-axis) and in focus (y-axis) at 620nm. **(b) Absorption map at 525nm of an arbitrary nanowire covered with a thick 1.36eV quantum dot layer** showing the higher absorption in the nanowire (yellow) compared to the quantum dots only (blue).

From this we conclude that the two systems interact optically, since the resonance changes. Also the absorption in the hybrid nanostructure increases. In Figure 5.6 (a) at resonance the absorption goes from 20% to 35%, a relative increase of about 60%. It can be argued that the extra absorption comes from absorption in the nanowire only. However in Figure 5.3 we see that the nanowire absorbs around 4% of the light at 550nm, so the additional absorption most likely stems from the absorption in the quantum dot shell as was seen from the intensity profiles in Figure 5.2. From FIB we found that the quantum dot layer on the nanowire was thinner than next to the nanowire, so we assume that the enhancement is even underestimated.

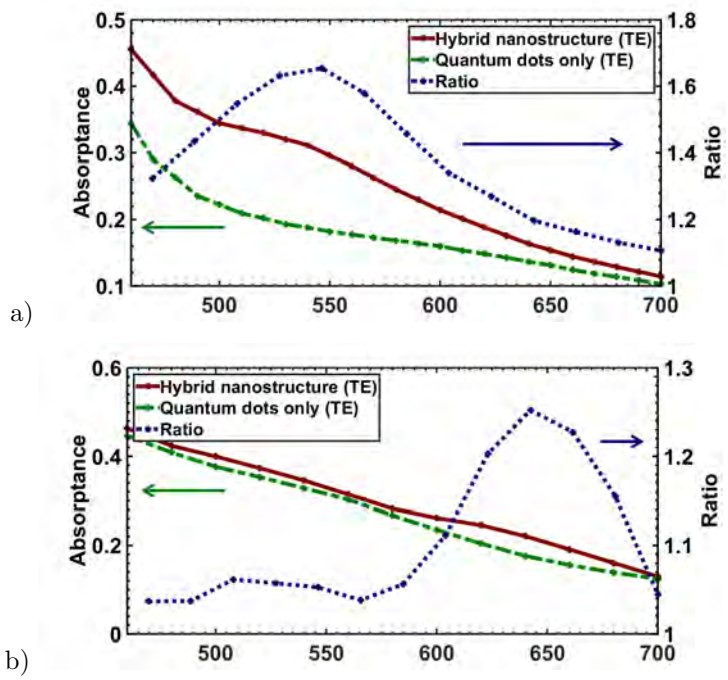

Figure 5.6: **Measured absorption signals** of (a) <20nm 0.61eV quantum dot shell on a nanowire compared to an only quantum dot film of 30nm and (b) A <50nm 1.36eV quantum dot shell on a nanowire compared to an only quantum dot film of 120-150nm. By dividing the two signals we find the ratio of absorption, showing a peak corresponding to a shifted resonance (right y-axis).

Near Infrared

The results in the previous Sections show that nanowires can enhance the absorption well beyond the range where they absorb strongly (<550nm). To emphasize this point, we measured the thick quantum dot layer sample in the infrared, where the nanowire absorption (without coverage) is well below 1%, even for thick nanowires. Two independent measurements (one in the 460nm-700nm wavelength range, one in the 700nm-1000nm wavelength range) on the same nanowire are done. The two signals are simply merged and show a perfect match, as can be seen in Figure 5.7. We see a factor of more than two between absorption in covered nanowires compared to only quantum dots at 790nm. It is worth noting that this is not the quantum dot absorption peak of the bandgap (at 910nm) but the absorption in the quantum dots enhanced by the redshifted resonance in the gold nanowire.

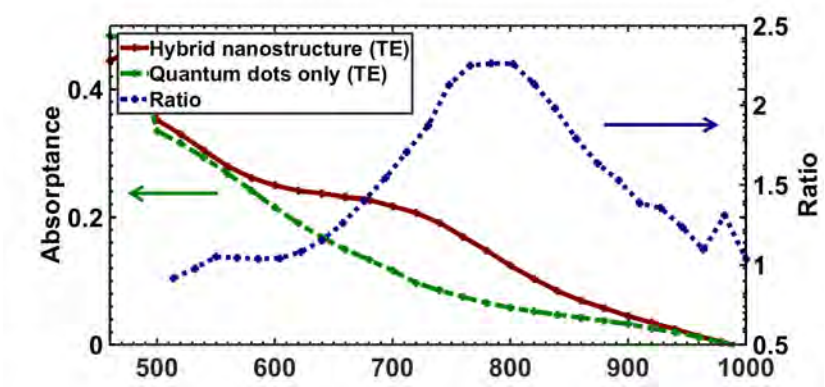

Figure 5.7: **Measured absorption signals of a nanowire covered with >50nm 1.36eV quantum dots and an only quantum dot film of about 120nm (left y-axis)**, both in the visible and the near infrared wavelength range. By dividing the two signals we find a ratio, showing a shifted resonance at around 790nm (right y-axis).

From multiple measurements, both with laser wavelenghts in the visible and the near-infrared we found resonances in the TE polarization. This resonance peak redshifts with increasing quantum dot layer thickness, as can be seen in Figure 5.8. The shift in resonance peak agrees with our estimated film thickness. Since from FIB images on all these samples we found that the quantum dot layer on the nanowire was thinner than next to the nanowire (which we measured with AFM) we could only estimate the quantum dot shell thickness on the nanowire, by comparing the absorption results with theoretical models and by using a tilt correction in FIB images.

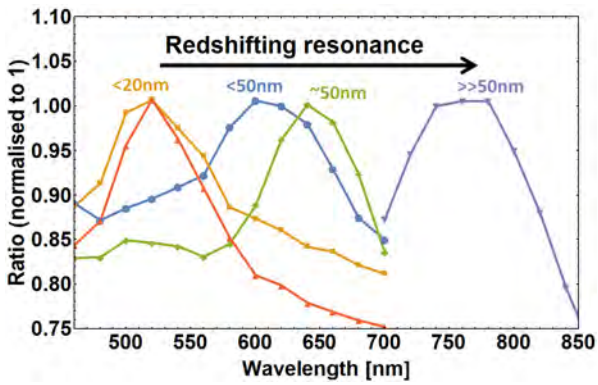

Figure 5.8: **Several ratios between the absorption in a nanowire covered with quantum dots, and in a quantum dot only film**, showing a redshifting resonance with increasing quantum dot film thickness. The peak is normalized to 1 for better comparison, but ranges between 1.3-2.5.

We also performed measurements on LbL covered nanowires that did not undergo a cleaning step, and thus most likely were still capped with long PVP chains. For a 3xLbL spincoated sample, we found a resonance in absorption at around 600nm. This was slightly lower than we found for the cleaned and functionalized nanowires. It remains unclear whether this difference is caused by the additional barrier layer (PVP), or by some other parameter like varied quantum dot on nanowire thickness. Although this result also implies an interaction between the two systems, the fact that the quantum dots are not directly linked to the nanowires but meet an insulating PVP barrier probably makes them electronically insulated, and thus not suitable for charge transfer.

5.3 Photoluminescence (PL) measurements

Photoluminescence emmission spectra were obtained from plasma-cleaned nanowires, functionalized with 12EDT and covered with a thick layer of 1.36eV quantum dots. This layer was around 150nm next to the nanowire (from AFM) and about 50nm on the nanowire (from FIB cross-section and comparison with theory). Only the bandgap of the 1.36eV quantum dots was in the detectable range of the PL setup, and thus no measurements were performed on smaller bandgap quantum dots. The samples were excited by a continuous wave laser at 532nm focused through a 100x objective. The excitation intensity was maintained at high lasing power (40μW) to assure detectable signal in the longer wavelength range. The setup allows for spatial scanning, where each pixel contains information on the emission per wavelength step.

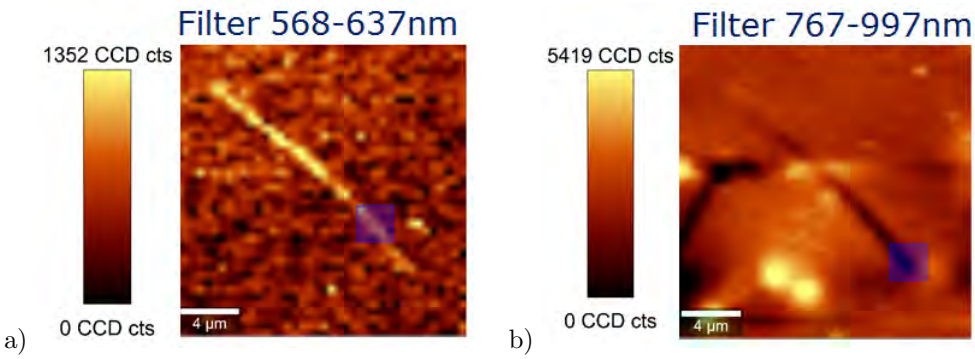

Figure 5.9: **Photoluminesce (PL) meaurements of a single nanowire covered with a 60nm LbL quantum dot layer with a bandgap of 1.36eV (910nm)** filtered between 568nm - 637nm (a) and 797nm - 997nm (b).

Figure 5.9 shows the counts of emission of two filtered wavelength ranges. In the 600nm wavelength range the sample showed more emission from the nanowire covered with quantum dots than from the surrounding quantum dots. Since the quantum dots do not emit at 600nm, we attribute the counts to noise in the detector and some broad emission, potentially from trapped states, that is enhanced on the nanowire due to better in- and outcoupling. We note that the countrate was very low despite more efficient detection in this wavelength range (Figure 5.9 (a)). When adding a filter at the bandgap wavelength of the quantum dots - here between 767-997nm - the counts of emission coming from the covered nanowire was less than from the surrounding quantum dots, as can be seen in Figure 5.9 (b). This decrease in emission might be attributed to quenching of the excited states on the quantum dots due to the presence of the nanowire, potentially due to charge transfer. We should not forget that the quantum dot layer on the nanowires is thinner than next to the nanowire, which may cause the difference in emission. Nevertheless, since the absorption measurement showed more absorption in the hybrid nanostructure compared to that in the surrounding quantum dots - which was even underestimated because the quantum dot layer on the nanowire was thinner - we would expect more emission from the nanowire (if the excitation was not quenched).

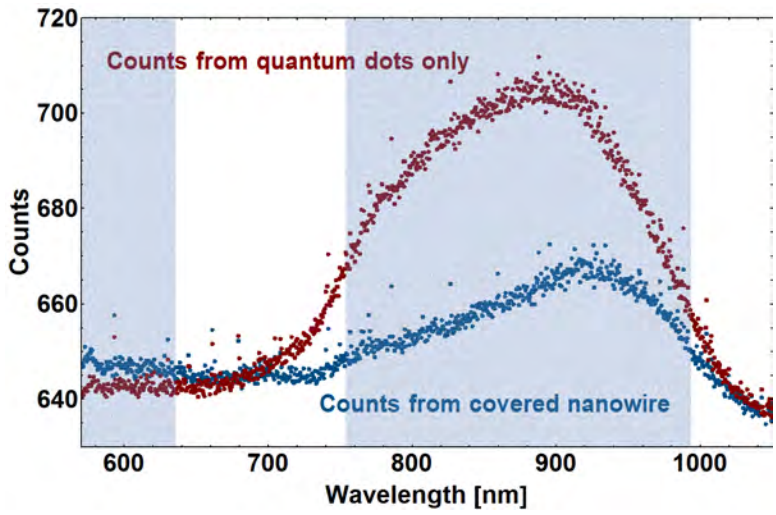

Figure 5.10: **Emission spectrum of nanowire covered with 1.36eV quantum dots (blue line) and of its surrounding quantum dots (red line)**. Shaded areas are the filtered areas. In the 767nm-997nm wavelength range, emission is higher from the surrounding quantum dots.

In Figure 5.9 (b) we find a dark area (no counts) on the left near the nanowire. When looking at optical images of the scanned area before and after scanning, we assume from the colorchange that the sample was damaged during scanning. The damaged area was used to focus the laser before the scan which means it received a high dose of radiation (see comparison between before and after scanning in Figures 5.11 (a) and (b)).

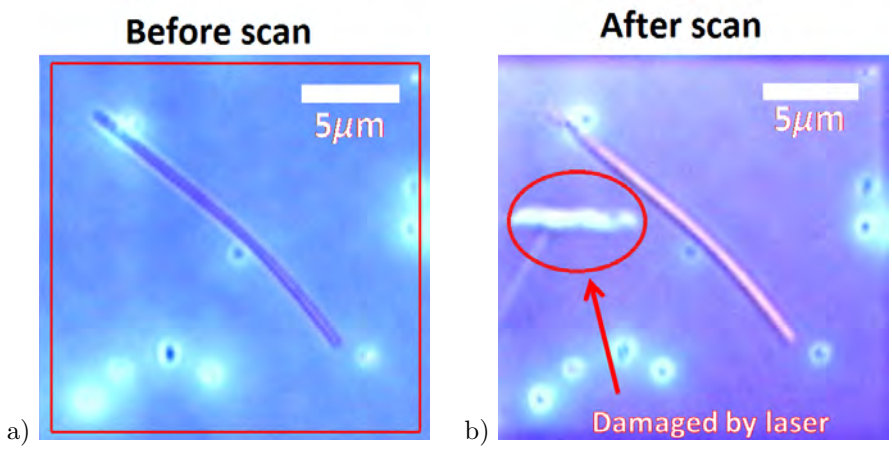

Figure 5.11: **Photoluminescence (PL) meaurements of a single nanowire covered with a 60nm LbL quantum dot layer with a bandgap of 1.36eV or 918nm.** (a) before scanning and (b) after scanning. It is clear that the scan damaged the sample, with a maximum where the laser was placed for focusing (red circle).

5.4 Note on the comparison between theory and experiment

We note that our theoretical calculations are based on cylindrical and infinitely long nanowires with a 100nm diameter, which is the average size of nanowires from the synthesis. Measurements were not necessarily done on 100nm nanowires, and the nanowires appeared to be less symmetric than hypothesized in the modeling (Figure 4.15 in the previous Chapter). The extinction coefficient for the quantum dots used for the core-shell model was based on fitted ellipsometry data of 1.25eV PbS quantum dots, whereas

most experiments were performed with 1.36eV quantum dots. The shell in the core-shell model was assumed to be smooth and homogeneous, whereas in reality the quantum dots are individual systems closely packed together. We do assume light to interact with the quantum dot layers as one effective medium, but still the surface of the layers is not smooth as is assumed in modeling. The ratio in the experimental data was obtained by dividing the absorption signal from the covered nanowires by the absorption signal from a quantum dot only film, which underestimates the hybrid nanostructure absorption because FIB and AFM showed the quantum dot layer on the nanowire to be thinner than the surrounding quantum dot film. The measurement is the sum of absorption in the quantum dot/nanowire hybrid nanostructure plus the absorption in the film of only quantum dots. This ratio (as comparison) is thus not so much quantitative, but qualitatively we show a good agreement between theory and measurements, as can be seen in Figure 5.12. For the quantum dot absorption, we used the Beer-Lambert law to get insight into the absorption, though scattering and thin-film interference effects were not considered here.

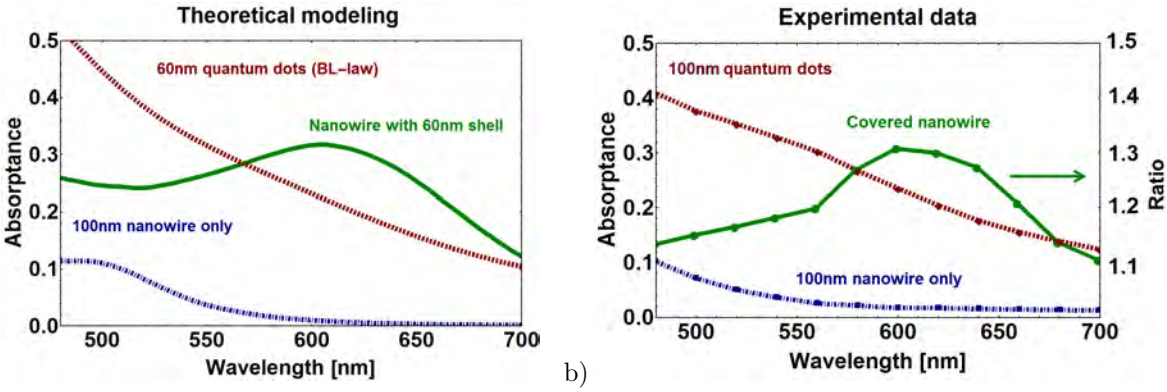

Figure 5.12: **Comparison between theory and experiment of an uncovered 100nm nanowire, a nanowire covered with a thick layer of quantum dots and absorption in a quantum dot film.** (a) Mie Theory was used for the nanowire modeling and the Beer-Lambert law to get insight into quantum dot absorption. (b) Data obtained from absorption measurements in the optics setup for a nanowire covered with <50nm of quantum dots on the nanowire and >100nm next to the nanowire (1.36eV). Note that Figure (b) has an extra y-axis on the right, showing the ratio of absorption in the hybrid nanostructure compared to the quantum dot only film.

5.5 Summary

Absorption measurements on single nanowires covered with quantum dots were performed. We found an increase in absorption on the nanowires when covered with quantum dots, and a shift of the resonance which redshifts with increasing quantum dot thickness. This absorption increase was most likely underestimated. The results are supported by theory, and from this we conclude that the nanowires and the quantum dots interact optically. Since the nanowires do not form a perfect core-shell hybrid nanostructure as in the theoretical model, no quantitative comparison could be done. However, the position of the resonance does compare with the theoretical predictions. From density field plots we found that the absorption enhancement is located in the shell covering the nanowire. Therefore we attribute the absorption increase to the quantum dot shell. In the near infrared - where plain nanowires absorb less than 1% - we found more than a doubling of absorption in the hybrid nanostructure compared to quantum dots only. Photoluminescence showed lower emission from the quantum dots when attached to the nanowires, which we attribute to quenching. This implies an electronic coupling, although this should be researched in more depth.

Chapter 6

Conclusions and Outlook

In this project a hybrid nanostructure was assembled by coating PbS quantum dots around gold nanowires. Nanowires and quantum dots were synthesized, and quantum dots were assembled on the nanowire both as a single layer shell and as a thick 'shell' by spincoating the quantum dots Layer-by-Layer onto nanowires. The connection between the two systems was facilitated by dithiols as linker molecules.

We have succesfully assembled a sub-monolayer coverage of quantum dots on nanowire surface. Both the nanowires and quantum dots were synthesized in solution. Nanowires were obtained in ethanol solution with very long PVP chains as capping agent, whereas PbS quantum dots were obtained in octane solution capped by oleic acid. Nanowires were dropcast on substrates, cleaned by plasma oxygen to remove the PVP - which seemed to block a direct ligand exchange to dithiols - functionalized in dithiol solution and placed in a quantum dot in octane solution. Then the substrates were cleaned thoroughly in octane, acetone an isopropanol to remove any unbound quantum dots. A nanowire coverage of at maximum 50% was achieved, with quantum dots attached to the nanowire and no quantum dots on the substrate, indicating successful binding to the nanowires. Mie Theory was used to model both the resonance and the electric field density in nanowires covered with quantum dots. This predicted a redshifting resonance with increasing quantum dot shell thickness and absorption enhancement inside this shell, which we confirmed by experiments. From theoretical modeling we found that a single layer would not show a clear absorption increase, so we introduced thick layers of quantum dots on the nanowires. By spincoating the quantum dots on the cleaned and functionalized nanowires Layer-by-Layer, we buried nanowires in quantum dots, obtaining a thick 'shell' of quantum dots around the nanowire of about 20nm - 150nm. A ligand exchange from long oleic acid chains to shorter 1,2-Ethanedithiol linker molecules facilitated better charge transport between quantum dots. FIB imaging and AFM gave insight into the layer thickness, showing quantum dot layers on the nanowire to be thinner than next to the nanowire.

We measured the absorption in these layer-by-layer covered nanowires. The comparison with theory was not quantitative, but as expected from modeling we found an increasing redshift in the resonance of the nanowire with increasing quantum dot shell thickness. From this redshift in resonance we conclude an optical interaction between the two nanostructures. Although the increased absorption in the visible wavelength range (460nm - 700nm) could still be (partly) attributed to absorption in the nanowire itself, the increased absorption both on and off resonance in the near infrared wavelength range (700nm - 1000nm) must be because of the interacting systems, since nanowires alone absorb less than 1% in this region.

From photoluminescence measurements we found a lower emission coming from the nanowire compared to the surrounding quantum dots, even though we had seen an absorption enhancement in the shell around the quantum dots. This lower emission can be attributed to quenching of quantum dot excitation possibly due to charge transfer. Since so far we have only probed one sample succesfully, more research must be done to confirm this interaction. The role of different dithiol linker molecules might as well be interesting in researching the electronic interaction between the nanowires and quantum dots.

In our hybrid nanostructure the plain gold nanowire resonates at 500nm, whereas the quantum dots have a bandgap at 910nm. Ideally to reach maximum absorption enhancement, a hybrid nanostructure is assembled with an overlap in nanowire resonance and quantum dot bandgap. This could be achieved by the use of a nanowire material that has a plasmon resonance at longer wavelengths, or by the use of smaller quantum dots with bandgaps at lower wavelengths. The Layer-by-Layer method in which

nanowires were buried in quantum dots resulted in interesting behaviour like redshifting resonances and absorption enhancement. This may also be a first step towards integration of nanowires into quantum dot layers, as a hybrid nanostructure in a plasmonically enhanced quantum dot solar cell.

These results suggest that this quantum dot/nanowire hybrid nanostructure may be a promising building block for photovoltaic applications. The structure is both optically and electronically highly tunable because materials can be changed, ligands can be varied, and sizes of both the quantum dot and nanowire can be altered in order to perfeclty match the solar spectrum. Since the metal nanowire allows for charge transport and can function as an electrode, introducing a second electrode would allow for charge collection. Research on the electronic interaction of the two nanostructures may give more insight in the actual application into photovoltaic devices.

Bibliography

[1] K. Catchpole, S. Mokkapati, F. Beck, W. E-C., A. McKinley, A. Basch, and J. Lee, *Plasmonics and nanophotonics for photovoltaics*, MRS Bulletin **36**, 461 (2011).

[2] A. Polman and H. Atwater, *Photonic design principles for ultrahigh-efficiency photovoltaics*, Nature Materials **11**, 174 (2012).

[3] G.-H. Kim, F. de Arquer, Y. Yoon, X. Lan, M. Liu, O. Voznyy, Z. Yang, F. Fan, A. Ip, P. Kanjanaboos, S. Hoogland, J. Kim, and E. Sargent, *High-Efficiency Colloidal Quantum Dot Photovoltaics via Robust Self-Assembled Monolayers*, Nano Letters **15 (11)**, 7691 (2015).

[4] S. Mann and E. Garnett, *Extreme light absorption in thin semiconductor films wrapped around metal nanowires*, Nano Letters **13 (7)**, 3173 (2013).

[5] S. Oener, S. Mann, B. Sciacca, C. Sfiligoj, J. Hoang, and E. Garnett, *Au-Cu2O core-shell nanowire photovoltaics*, Applied Physics Letters **106**, 023501 (2015).

[6] B. Sciacca, S. Mann, F. Tichelaar, H. Zandbergen, M. van Huis, and E. Garnett, *Solution-phase epitaxial growth of quasi-monocrystalline cuprous oxide on metal nanowires*, Nanoletters **14 (10)**, 5891 (2014).

[7] B. Ehrler, *Nanocrystalline Solar Cells*, PhD thesis, University of Cambridge, 2012.

[8] C.-H. Chuang, P. Brown, V. Bulovic, and M. Bawendi, *Improved performance and stability in quantum dot solar cells through band alignment engineering*, Nature materials **13**, 796 (2014).

[9] J. Twidell and T. Weir, *Renewable Energy Sources*, Taylor and Francis, 2006.

[10] E. Garnett, M. Brongersma, Y. Cui, and M. McGehee, *Nanowire Solar Cells*, Annual Review Material Research **41**, 269 (2011).

[11] P. Wurfel, *Physics of Solar Cells*, Wiley, 2009.

[12] J. Tang and E. Sargent, *Infrared Colloidal Quantum Dots for Photovoltaics: Fundamentals and Recent Progress*, Advanced Materials **23**, 12 (2011).

[13] H. Atwater and A. Polman, *Plasmonics for improved photovoltaic devices*, Nature Materials **9**, 205 (2010).

[14] J. Luther, M. Law, Q. Song, C. Perkins, M. Bear, and A. Nozik, *Structural, Optical, and Electrical Properties of Self-Assembled Films of PbSe Nanocrystals Treated with 1,2-Ethanedithiol*, ACS Nano **2**, 271 (2008).

[15] V. Klimov, *Semiconductor and Metal Nanocrystals: Synthesis and Electronic and Optical Properties*, CRC Press, 2003.

[16] I. Moreels, K. Lambert, D. Smeets, D. de Muynck, T. Nollet, J. Martins, F. Vanhaecke, A. Vantomme, C. Delerue, G. Allan, and Z. Hens, *Size-Dependent Optical Properties of Colloidal PbS Quantum Dots*, ACS Nano **3 (10)**, 3023 (2009).

[17] A. Bakulin, S. Neutzner, H. Bakker, L. Ottaviani, D. Barakel, and Z. Chen, *Charge Trapping Dynamics in PbS Colloidal Quantum Dot Photovoltaic Devices*, ACS Nano **7**, 8771 (2013).

[18] J. Tang and E. Sargent, *Colloidal-quantum-dot photovoltaics using atomic-ligand passivation*, Nature Materials **10**, 765 (2011).

[19] P. Smowton, E. Hermann, Y. Ning, H. Summers, P. Blood, and M. Hopkinson, *Optical mode loss and gain of multiple-layer quantum-dot lasers*, Applied Physics Letters **78**, 2629 (2001).

[20] J. van de Groep, D. Gupta, M. Verschuuren, M. Wienk, R. Janssen, and A. Polman, *Large-area soft-imprinted nanowire networks as light trapping transparent conductors*, Science **5** (2015).

[21] W. Shockley and H. Queisser, *Detailed Balance Limit of Efficiency of pn Junction Solar Cells*, Journal of Applied Physics **32**, 510 (1961).

[22] R. Schaller and V. Klimov, *High efficiency carrier multiplication in PbSe nanocrystals: implications for solar energy conversion*, Physical Review Letters **92**, 186601 (2004).

[23] M. Beard, J. Luther, O. Semonin, and A. Nozik, *Third generation photovoltaics based on multiple exciton generation in quantum confined semiconductors*, Accounts of chemical research **46**, 1252 (2013).

[24] O. Semonin, J. Luther, S. Choi, Y.-H. Chen, J. Gao, A. Nozik, and M. Beard, *Peak External photocurrent Quantum*

Efficiency Exceeding 100percent via MEG in a Quantum Dot Solar Cell, Science **334**, 1530 (2011).

[25] J. Sambur, T. Novet, and B. Parkinson, *Multiple exciton collection in a sensitized photovoltaic system*, Science **330**, 63 (2010).

[26] J. Schuller, E. Barnard, W. Cai, Y. Jun, J. White, and M. Brongersma, *Plasmonics for extreme light concentration and manipulation*, Nature Materials **9**, 193 (2010).

[27] S. Maier and H. Atwater, *Plasmonics: Localization and guiding of electromagnetic energy in metal/dielectric structures*, Journal of Applied Physics **98**, 011101 (2005).

[28] L. Cao, J. White, J.-S. Park, J. Schuller, B. Clemens, and M. Brongersma, *Engineering light absorption in semiconductor nanowire devices*, Nature Materials **8**, 643 (2009).

[29] D. Hecht, H. L., and G. Irvin, *Emerging Transparent Electrodes Based on Thin Films of Carbon Nanotubes, Graphene, and Metallic Nanostructures*, Advanced Materials **23**, 1482 (2011).

[30] D. Seo, J. Park, J. Jung, S. Park, S. Ryu, and H. Song, *One-Dimensional Gold Nanostructures through Directed Anisotropic Overgrowth from Gold Decahedrons*, J.Phys.Chem **113 (9)**, 3449 (2009).

[31] Y. Zhan, J. Zhao, C. Zhou, M. Alemayehu, Y. Li, and Y. Li, *Enhanced photon absorption of single nanowire a-Si solar cells modulated by silver core*, Optics express **20**, 158 (2012).

[32] D. Barber and I. Freestone, *An Investigation of the Origin of the Colour of the Lycurgus Cup by Analytical Transmission Electron Microscopy*, Archaemetry **32**, 33 (1990).

[33] W. Hergert and T. Wriedt, *The Mie Theory: Basics and Applications*, Springer, 2012.

[34] C. Bohren and D. Huffman, *Absorption and Scattering of Light by Small Particles*, Wiley, 2008.

[35] E. Palik, *Handbook of Optical Constants of Solids, Vol. 1*, Academic: New York, 1998.

[36] J. Love, L. Estroff, J. Kriebel, R. Nuzzo, and G. Whitesides, *Self-assembled monolayers of thiolates on metals as a form of nanotechnology*, Chem Rev **105 (4)**, 1103 (2005).

[37] D. Norris, M. Bawendi, and L. Brus, *Optical properties of semiconductor nanocrystals (quantum dots)*, Molecular Electronics , 281 (1997).

[38] J. Zhang, J. Gao, E. Miller, J. Luther, and M. Beard, *Diffusion-Controlled Synthesis of PbS and PbSe Quantum Dots with in Situ Halide Passivation for Quantum Dot Solar Cells*, ACS Nano **8**, 614 (2014).

[39] J. Zhang, W. Sun, L. Yin, X. Miao, and D. Zhang, *One-pot synthesis of hydrophilic CuInS2 and CuInS2ZnS colloidal quantum dots*, Journal of Materials Chemistry **24**, 4812 (2014).

[40] L. Yang, M. Tabachnyk, S. Bayliss, M. Bohm, K. Broch, N. Greenham, R. Friend, and B. Ehrler, *Solution-Processable Singlet Fission Photovoltaic Devices*, Nano Letters **15 (1)**, 354 (2015).

[41] D. Seo, C. Yoo, I. Chung, S. Park, S. Ryu, and H. Song, *Shape adjustment between multiply twinned and single-crystalline polyedral gold nanocrystals: decahedra, icosahedra, and truncated tetrahedra*, J.Phys.Chem **112 (7)**, 2469 (2008).

[42] J. Luther, M. Law, M. Beard, Q. Song, M. Reese, R. Ellingson, and A. Nozik, *Schottky solar cells based on colloidal nanocrystal films*, Nano letters **8 (10)**, 3488 (2008).

[43] P.-A. A.G., I. Kramer, A. Barkhouse, X. Wang, G. Konstantatos, R. Debnath, L. Levina, I. Raabe, M. Nazeeruddin, M. Gratzel, and E. Sargent, *Depleted-heterojunction colloidal quantum dot solar cells*, ACS Nano **4 (6)**, 3374 (2010).

[44] S. Mann, B. Sciacca, J. Wang, and E. Garnett, *Integrating sphere microscopy for quantitative absorption measurements of single scattering nanoparticles*, Under review (2015).

[45] J.-J. Zhu, C.-X. Kan, J.-G. Wan, M. Han, and G.-H. Wang, *High-Yield Synthesis of Uniform Ag Nanowires with High Aspect Ratios by Introducing the Long-Chain PVP in an Improved Polyol Process*, Journal of Nanomaterials (2011).

[46] Y.-J. Song, M. Wang, X.-Y. Zhang, J.-Y. Wu, and T. Zhang, *Investigation on the role of the molecular weight of polyvinyl pyrrolidone in the shape control of high-yield silver nanospheres and nanowires*, Nanoscale Research Letters **13**, 9 (2014).

[47] F. Pietra, F. Rabouw, P. van Rhee, J. van Rijssel, A. Petukhov, B. Ern, P. Christianen, C. de Mello Doneg, and D. Vanmaekelbergh, *Self-assembled CdSe/CdS nanorod sheets studied in the bulk suspension by magnetic alignment.*, ACS Nano **8 (10)**, 10486 (2014).